Earth and Space Science

RESEARCH ARTICLE
10.1029/2023EA003009

Key Points:

- We investigated maar-diatreme structure of the new Pleistocene Bažina maar in the western Eger Rift by combined geophysical and drilling research
- Geophysical methods verified the maar origin, lithologies from two boreholes revealed volcanic rocks with basaltic feeding conduit
- Our multidisciplinary approach disclosed several generations of eruptions leading to a formation of another scoria cone within the maar

Supporting Information:

Supporting Information may be found in the online version of this article.

Correspondence to:

P. Hrubcová,
pavla@ig.cas.cz

Citation:

Hrubcová, P., Fischer, T., Rapprich, V., Valenta, J., Táborík, P., Mrlina, J., et al. (2023). Two small volcanoes, one inside the other: Geophysical and drilling investigation of Bažina maar in western Eger Rift. *Earth and Space Science*, *10*, e2023EA003009. https://doi.org/10.1029/2023EA003009

Received 3 MAY 2023
Accepted 27 JUN 2023

Author Contributions:

Conceptualization: Pavla Hrubcová, Tomáš Fischer, Vladislav Rapprich, Torsten Dahm
Data curation: Pavla Hrubcová, Vladislav Rapprich, Jan Valenta, Petr Táborík, Jan Mrlina, Tomáš Vylita, Roman Beránek, Radek Klanica, Josef Vlček, Veronika Turjaková

Two Small Volcanoes, One Inside the Other: Geophysical and Drilling Investigation of Bažina Maar in Western Eger Rift

Pavla Hrubcová[1], Tomáš Fischer[2], Vladislav Rapprich[3], Jan Valenta[2], Petr Táborík[2], Jan Mrlina[1], Torsten Dahm[4,5], Tomáš Vylita[2], Roman Beránek[1], Radek Klanica[1], Josef Vlček[2], and Veronika Turjaková[1]

[1]Institute of Geophysics, Czech Academy of Sciences, Prague, Czech Republic, [2]Faculty of Science, Charles University in Prague, Prague, Czech Republic, [3]Czech Geological Survey, Prague, Czech Republic, [4]GFZ German Research Centre for Geosciences, Potsdam, Germany, [5]University of Potsdam, Potsdam, Germany

Abstract Maar-diatreme volcanoes are small volcanic structures with a funnel-shaped crater surrounded by a tephra-ring. They are usually formed by the explosive phreatomagmatic eruptions when groundwater comes into the contact with magma. We focus on such a structure in the geodynamically active western Eger Rift (Czech Republic) and present results from multidisciplinary geophysical investigation calibrated by drilling in the newly discovered Pleistocene Bažina maar. We evaluated morphological (LiDAR-based DEM) data and confirmed the existence of a maar-diatreme structure by combined geophysical methods. In the map view, they revealed circular negative gravity anomaly, funnel-shape low-resistivity anomaly, and strong magnetic anomaly. These results allowed for the optimal location of two boreholes in the maar crater, which evinced its contact with country rocks and lithologies of the maar-diatreme filling. The drilling revealed coherent volcanic rocks and volcaniclastic deposits, moreover, it revealed a presence of a pyroclastic cone with the olivine nephelinite feeding conduit. Further investigations disclosed maar structure and subsequent pyroclastic cone(s) with several generations of eruptions and systematic decrease of water influence on the eruption style. Different eruption styles suggest a unique evolution of two volcanoes, one inside the other. The age of the Bažina maar eruption, estimated from the reverse polarity of the detected magnetic anomaly, implies that the effusion and solidification of the lava during the eruption must be older than 0.78 Ma (Pleistocene). This points to an active volcanism in the western Eger Rift in a span of ~0.5 Ma, where Bažina represents the oldest (maybe opening) phase.

Plain Language Summary Maars are small volcanoes formed by the explosive eruptions when water comes into the contact with magma. They can form topographic depressions, however, their discovery is not easy and they can be easily missed in the fields. We focused on a newly discovered depression Bažina in the western Eger Rift (Czech Republic), which was supposed to be such a maar. Combination of geophysical surveys and drilling revealed small volcano with a complex structure. Geophysical results proved its magmatic origin and allowed for the optimal location of two exploration boreholes. They evinced the maar contact with the country rocks, coherent volcanic rocks and volcaniclastic deposits with basaltic conduit. Further investigations disclosed several subsequent eruptions within the maar with different eruption styles, from maar-forming eruption to Surtseyan style eruption and finally to Strombolian style eruption. These different eruption styles suggest the unique evolution of two volcanoes, one inside the other. The schematized animated history of this volcano is accessible at https://www.youtube.com/watch?v=VxhFrM6WR8c.

1. Introduction

Maar-diatreme volcanoes are produced by the explosive eruptions that cut deeply into the country rocks and form broad flat-floored craters surrounded by low-relief tuff rings. They are generally accepted to be formed by the explosive phreatomagmatic eruptions in a short time, which occur as a result of a violent expansion of magmatic gas or steam, or when groundwater comes into the contact with hot lava or magma. These eruptions are usually episodic, continuously propagating downwards and enlarging the crater (e.g., Lorenz & Kurszlaukis, 2007). Structurally, they consist of a flat-floored maar crater surrounded by an ejecta ring, and a downward propagating diatreme filled with pyroclastic breccia (White & Ross, 2011). The maar crater is commonly filled with water and forms an oval lake, as is the case of many maars, for example, in the Eifel mountains in Germany (Sirocko

Formal analysis: Jan Valenta, Petr Táborík, Jan Mrlina, Roman Beránek, Radek Klanica
Funding acquisition: Pavla Hrubcová, Tomáš Fischer, Torsten Dahm
Investigation: Pavla Hrubcová, Tomáš Fischer, Vladislav Rapprich
Project Administration: Pavla Hrubcová, Tomáš Fischer, Torsten Dahm
Supervision: Pavla Hrubcová, Tomáš Fischer, Tomáš Vylita
Validation: Pavla Hrubcová, Tomáš Fischer
Visualization: Vladislav Rapprich, Jan Valenta, Jan Mrlina, Roman Beránek, Radek Klanica
Writing – original draft: Pavla Hrubcová, Vladislav Rapprich, Jan Valenta, Jan Mrlina
Writing – review & editing: Pavla Hrubcová, Tomáš Fischer, Vladislav Rapprich

et al., 2013). However, the maar can also be dry, which arises when water supply for the lake is not available, maar lake dries out or becomes sediment-filled (e.g., Sirocko et al., 2013; White, 1990).

In contrast to other types of volcanoes, maar craters do not form edifices significantly rising above surrounding landscape. Instead, funnel-shaped crater rimmed with easily removable tephra-ring is created (e.g., Lorenz & Kurszlaukis, 2007). For this reason, their detection is much more complicated and they can be easily missed in the fields. This is especially the case when the tuff ring surrounding the crater is eroded and/or the maar crater is completely filled with post-eruptive sediments of any type. While the internal structure of other monogenetic volcanoes can be revealed by erosion or quarrying (e.g., Foucher et al., 2018; Hintz & Valentine, 2012; Keating et al., 2008; Petronis et al., 2013, 2018), the rock sequences of the maar infill can be more blurred due to their less coherent and more erodible nature compared to country rocks. In the case of older (pre-Pliocene) maar-diatreme volcanoes, the subsequent erosion of the surrounding country rocks may expose the diatreme facies, but usually without maar-filling sequences (e.g., Latutrie & Ross, 2019, 2021; Lefebvre et al., 2013; Skácelová et al., 2010; Valenta et al., 2014). In some cases, the maar facies can be represented by a solidified lava-lake, preventing the diatreme rocks from erosion (e.g., Latutrie & Ross, 2020). Knowledge of the evolution of the maar-diatreme volcanoes, namely those of Quaternary age and the ones not affected by the erosion, is therefore highly dependent on geophysical research (Barde-Cabusson et al., 2013; Bolós et al., 2012; Brunner et al., 1999; Flechsig et al., 2015; Mrlina et al., 2009; Oms et al., 2015; Skácelová et al., 2010). Drilling investigations upgrade our knowledge; however, they are usually limited to lacustrine sequences in the maar-crater filling (Läuchli et al., 2021; Mrlina et al., 2009; Peti & Augustinus, 2019; Zolitschka et al., 2013) and therefore not comprehensive enough to provide the whole picture.

Occasionally, continuing magma supply persisting after the maar eruption may lead to a formation of a maar-hosted lava-lake, as is the case of the Hopi Buttes Volcanic Field in Arizona (Latutrie & Ross, 2020). If the feeder migrates, it may lead to a composite maar(s)/tuff-cone complex as in Jeju Island, South Korea (Sohn & Park, 2005). It can also create a scoria cone at the maar edge as in case of the Lunar Crater Volcanic Field, Nevada (Amin & Valentine, 2017). More rarely, it can also create a scoria cone within the crater itself (El Jagüey-La Breña complex, Mexico: Swanson, 1989; Pula maar, Hungary: Németh et al., 2008; Pali Aike Volcanic Field, Argentina: Ross et al., 2011; Auckland Volcanic Field, New Zealand: Németh et al., 2012; Meke maar, Turkiye: Güllü & Kadıoğlu, 2019). They provide valuable insight into the processes forming a maar nested with scoria-cone. However, sometimes their possibilities are limited; especially in case of maar-hosted scoria cones with investigations confined to morphology and/or superficially exposed pyroclastic sequences.

Some windows into the internal structure of the maar hosting a scoria cone can be provided by partly eroded volcanic fields. Valentine and van Wyk de Vries (2014) described the Mardoux diatreme structure in Gergovie (France) with intrusions suggesting the original presence of pyroclastic cones on the top of the diatreme inside the maar; however, they did not find any evidence of the scoria cone in the eroded diatreme. The Oligocene Luž/Lausche volcano at the border among the Czech Republic, Poland, and Germany revealed a scoria cone inside the maar where the hosting maar was in later phase protruded by a phonolite lava dome, significantly obscuring the maar-scoria cone settings and relationships (Wenger et al., 2017). However, there are still open questions related to such pyroclastic cone successions and their evolution within the maar-crater.

In this paper, we shed more light on the evolution of the maar-hosted pyroclastic cones. We present an image of a maar-diatreme volcano hosting a set of pyroclastic cones, which was newly discovered at the western flank of the Cheb Basin in the western Eger Rift (Czech Republic at the border with Germany). It sits in the intra-continental geodynamic area (Figure 1), where the activity is manifested by mid-crustal earthquake swarms, massive diffuse degassing of mantle-derived CO_2 (e.g., Bräuer et al., 2003; Fischer et al., 2017, 2020) and Cenozoic volcanism at the intersection of the western Eger Rift with major intraplate faults and tectonic zones (Ulrych et al., 2011). The volcanism is of intraplate alkaline character and is documented in two Quaternary scoria cones and series of maars. Two of these maars (Ztracený rybník and Bažina; Figure 1) were newly discovered based on the evaluation of the morphological data (LiDAR-based DEM) and ground geophysical investigation (Hošek et al., 2019; Mrlina et al., 2019). In this paper, we focus on the Bažina maar and discuss results from multidisciplinary geophysical investigations calibrated by drilling in the frame of the ICDP Eger project (International Continental Drilling Program; Fischer et al., 2022). Apart from the internal structure, we show how detailed pre-drill geophysical research contributed to a proper selection of the drill site, which concluded in revealing the unique structure of a maar volcano with several generations of eruptions. Such results not only improve our understanding of volcanic processes but also shed light on tectonic evolution at the western margin of the Eger Rift.

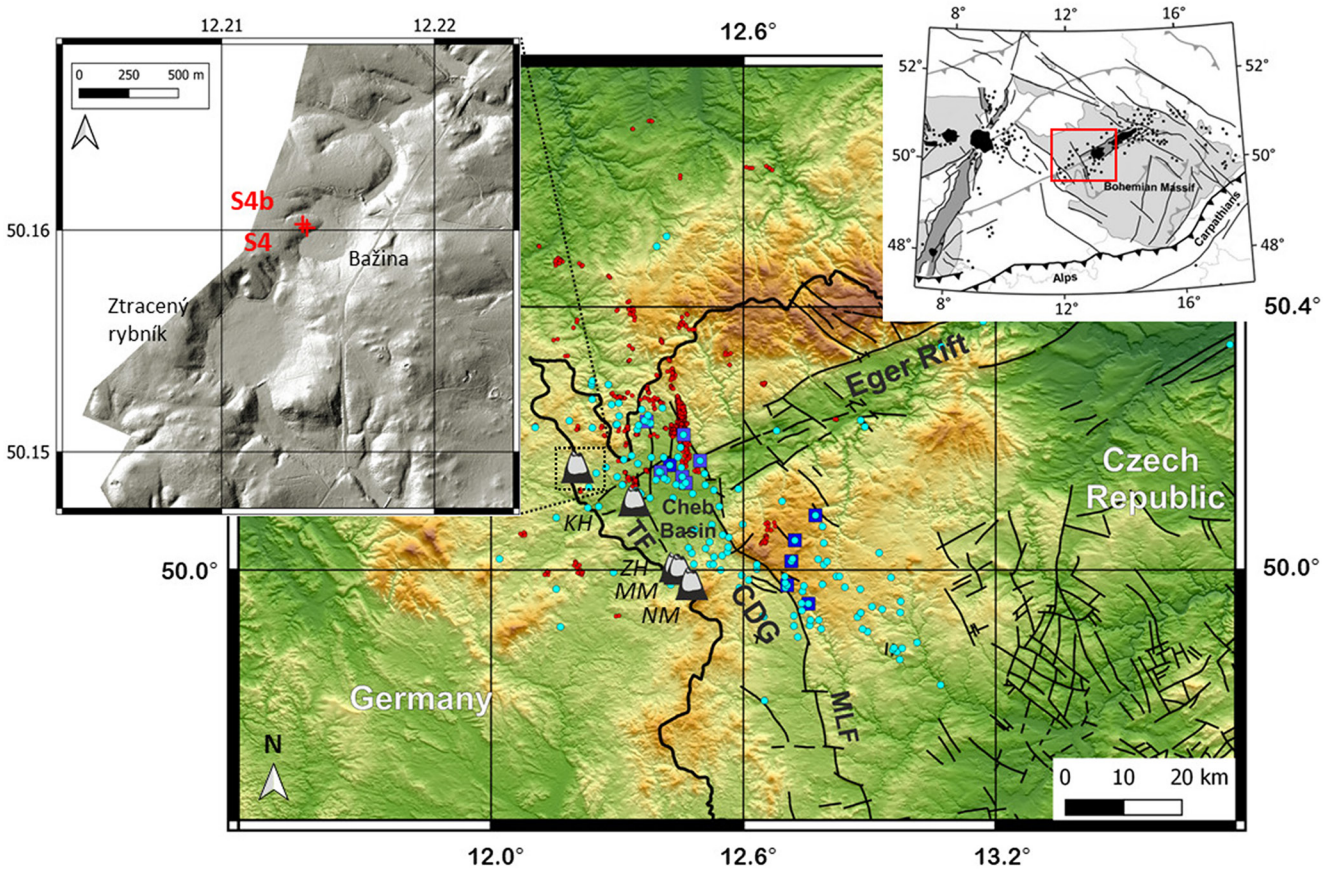

Figure 1. The West Bohemia geodynamic region with the Cheb Basin at the intersection of the Eger Rift and the Cheb-Domažlice Graben (CDG). TF, Tachov Fault; MLF, Mariánské-Lázně Fault. The earthquakes (red circles), CO_2 degassing (cyan circles), and mofettes (blue squares) indicated together with the position of six Quaternary volcanoes (NM, Neualbenreuth maar; MM, Mýtina maar; ZH, Železná hůrka and KH, Komorní hůrka scoria cones). The inset (top left) shows the zoomed part of two newly discovered maar-diatreme volcanoes (Ztracený rybník and Bažina) based on LiDAR-DEM data (DMR 5G, https://geoportal.cuzk.cz). The inset (top right) shows the Cenozoic volcanism (in black) in central Europe (after Ulrych et al., 2011) with the red rectangle indicating the West Bohemian region.

2. Tectonic Setting

The Cenozoic alkaline intraplate volcanism of the Bohemian Massif, the easternmost termination of the Variscan orogenic belt in central Europe, belongs to the Central European Volcanic Province (CEVP; Wilson & Downes, 1991). It forms an arc-shaped belt, which extends from the western to the easternmost parts of the massif. The most prominent western segment is associated with the NE-SW trending Eger Rift (Prodehl et al., 1995), which is considered to be a reactivated Variscan suture zone separating lithospheric domains: the Saxothuringian in the NW from the Moldanubian and Teplá-Barrandian in the SE (Babuška & Plomerová, 2001). Such a reactivation indicates a structural control on the Cenozoic volcanic activity (Babuška et al., 2010) with magmatic rocks compositionally similar to rocks from other parts of the CEVP in range from melilitites, basanites, alkali basalts and possibly carbonatites to evolved rock types such as phonolites and trachytes (Ulrych et al., 2011).

The Cenozoic magmatic activity of the Bohemian Massif lasted from the Late Cretaceous until the Middle Pleistocene (Ulrych et al., 2011) with the climax during the Oligocene–Lower Miocene (Büchner et al., 2015; Holub et al., 2010; Skála et al., 2014; Ulrych et al., 2003). During this time, the alkaline magmas erupted mainly along the NE-SW trending suture between the Saxothuringian and Teplá-Barrandian domains of the Bohemian Massif (Mlčoch & Konopásek, 2010) with significantly smaller magma batches erupted aside this zone. After the termination of the main volcanic phase during the Miocene, the Eger Rift (Figure 1) was subject to the extension and subsidence along the same NE-SW trending Variscan suture zone (Rajchl et al., 2009). The opening of the Eger Rift was accompanied by a decrease in volcanic activity and its shift to the rift shoulders (Rapprich et al., 2007; Ulrych et al., 2016).

The following evolution of the Bohemian Massif during the Pliocene and Pleistocene was characterized by significant re-distribution of tectonic and volcanic activity (e.g., Rajchl et al., 2009; Ulrych et al., 2011). The prominent tectonic feature of this period was a system of NW-SE to NNW-SSE trending left-lateral faults, almost perpendicular to the Eger Rift, crosscutting the Bohemian Massif at various segments. In the eastern margin of the Bohemian Massif, the Marginal Sudetic Fault was associated with Early Pleistocene (Gelasian) Bruntál volcanic field (Cajz et al., 2012). In the northern part of the Bohemian Massif, the Pliocene reactivation of the Lusatian overthrust was associated with the reactivation of the Jičín Volcanic Field (Cajz et al., 2009). Finally, the NNW-SSE transtensional Cheb-Domažlice Graben (CDG) opened near the western margin of the Bohemian Massif. The CDG hosts the Cheb Basin (Figure 1), which initiated in the Eocene, continued during the Eger Rift opening and rejuvenated with the activation of the CDG (Špičáková et al., 2000). The area is also weakened due to a triple junction of three lithospheric domains of the Bohemian Massif (Babuška et al., 2007).

The CDG is delimited by two fault systems, the Mariánské Lázně Fault (MLF) zone in the east (Fischer et al., 2012) and the Tachov Fault (TF) in the west (Figure 1). Both systems differ in the expression of the Pleistocene-Holocene activity. The MLF is associated with a massive diffuse degassing of mantle-derived CO_2 (Bräuer et al., 2003, 2008) and with a periodic occurrence of the earthquake swarms (Fischer et al., 2014; Horálek & Fischer, 2008), but without signs of the post-Miocene volcanic activity. The TF exhibits less recent seismicity; however, this fault is associated with several Pleistocene volcanoes (e.g., Ulrych et al., 2003). Fluid degassing of CO_2 in the Cheb Basin and surrounding areas is in the form of wet and dry mofettes, and mineral springs. They comprise high portions of mantle-derived helium and CO_2, which indicate mantle origin and fluid transport from the depleted lithospheric mantle (Bräuer et al., 2009; Muñoz et al., 2018; Platz et al., 2022; Weinlich et al., 1999), possibly with imprints at the crust-mantle boundary (Hrubcová & Geissler, 2009; Hrubcová et al., 2005, 2013, 2017).

We focus on the volcanic activity along the TF with several Pleistocene volcanoes (Figure 1). Two scoria cones Komorní hůrka/Kammerbühl (KH) and Železná hůrka/Eisenbühl (ZH) have been known since the 18th century (e.g., Gottsmann, 1999; Hradecký, 1994; Rapprich et al., 2019), while the other Pleistocene volcanoes in this area remained undisclosed until the last two decades. First, the Mýtina maar near ZH scoria cone was disclosed in the Czech Republic (Mrlina et al., 2009), followed by the Neualbenreuth maar in Germany (Rohrmüller et al., 2018), both penetrating phyllites of the Dyleň massif. The age of their eruption was determined from Ar-Ar geochronology to the Mid Pleistocene, at 0.27–0.29 Ma (Mrlina et al., 2009; Rohrmüller et al., 2018). More recently, twin maars Ztracený rybník and Bažina in the northern segment of the TF zone in the Czech Republic were recognized (Hošek et al., 2019; Mrlina et al., 2019), both penetrating granites of the Smrčiny batholith.

3. Data and Methods

3.1. Geomorphology From LiDAR-Based Data

We started our research with inspecting the geomorphology. New airborne laser imaging (LiDAR) carried out on the territory of the Czech Republic during 2013–2016 resulted in the Digital Model of the Relief of the Czech Republic of the 5th Generation (DMR 5G). These data with their regular updates are accessible through the web interface (https://geoportal.cuzk.cz) and provide the elevations (Baltic referenced) with the mean error of 0.18 m in an open landscape and of 0.3 m in a forest area. They represent a source data set for creating contour maps of a high level of detail.

A close inspection of these morphological data around the Cheb Basin enabled us to discover two new circular depressions, Ztracený rybník and Bažina (Figure 1). They both were suspected to originate from a maar-forming eruption. To confirm that, we further investigated them by ground geophysical surveying, and later by drilling.

3.2. Geophysical Investigations

First, these twin circular morphological depressions Ztracený rybník and Bažina (Figure 1) were examined by ground gravimetry and magnetometry as relatively fast and operational reconnaissance surveys. The gravity measurements helped to verify the origin of the morphological depressions and their possible relation to a maar structure. The magnetometry targeted possible mafic feeder dikes or lava accumulations. The ground resistivity measurements interpreted by the electrical resistivity tomography (ERT) method disclosed further details of the maar filling and its contact with the country rocks. Results of these combined geophysical investigation confirmed maar origin of both depressions; however, it also disclosed their differences. Whereas the Ztracený

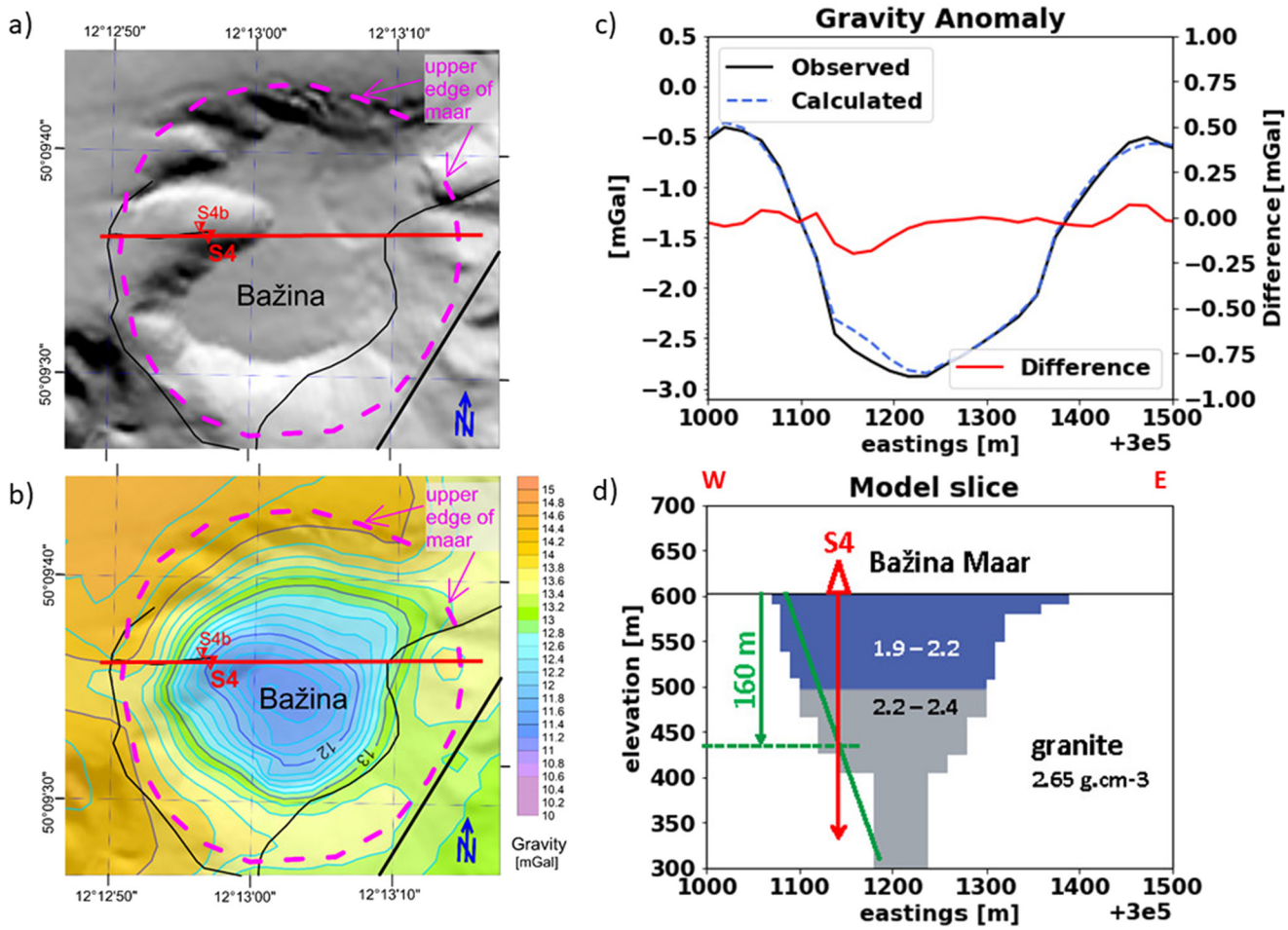

Figure 2. (a) The morphology (LiDAR-based DEM) of the Bažina maar. (b) The Complete Bouguer anomaly. Note the relative negative anomaly of −2.8 mGal (blue color) with the minimum at 11.2 mGal, delimited by the 14 mGal contour-line coinciding with the circular shape of the morphological depression. The expected upper edge of the maar (diameter of 300 m) is indicated by violet dashed line; red line indicates the modeling section; the position of drill holes S4 and S4b also indicated. (c) Gravity modeling along the W-E section. The anomaly with the observed and calculated gravity. The red curve represents the difference between the observed and calculated values. (d) The density model (in g/cm^3) of the Bažina maar along the EW profile. The green line is the approximation of the maar wall dipping at 69° from horizontal; the S4 drill hole cuts this modeled maar wall at 160 m depth.

rybník maar displayed relatively simple electrical resistivity image and the absence of magnetic anomaly, the data from the Bažina maar revealed strong magnetic anomaly and suggested more complex setting. For these reasons, in our research, we focused on the Bažina maar.

3.2.1. Gravity Measurements

The gravity measurement was performed with the Scintrex CG-6 and LaCoste-Romberg D gravimeters supported by GNSS and total station surveying. In the Bažina maar, the survey comprised 90 gravity high-resolution points measured with the accuracy of 0.012 mGal for the observed gravity and the accuracy of 0.05 m for the elevation (Mrlina et al., 2019). The processing involved terrain corrections and resulted in the Complete Bouguer anomalies. They were interpolated by the kriging procedure (Mrlina et al., 2019), and plotted with the Surfer program package (Golden Software) (Figure 2). The resulting anomalous gravity was negative and coincided with the oval shape of the morphological depression. Its almost isometric shape has a diameter of about 300 m with a small extension toward NE where the maar depression opens into a small brook. The Complete Bouguer anomaly minimum of 11.2 mGal (Figure 2b) represents the relative negative anomaly of −2.8 mGal (Figure 2c) delineating the extent of low-density rocks, mainly maar sediments and volcaniclastic deposits.

The Complete Bouguer anomalies (Figure 2b) served as the input for the 3D forward-inverse gravity modeling (Figures 2c and 2d). The density model of the maar-diatreme structure was inverted from the gravity data in a

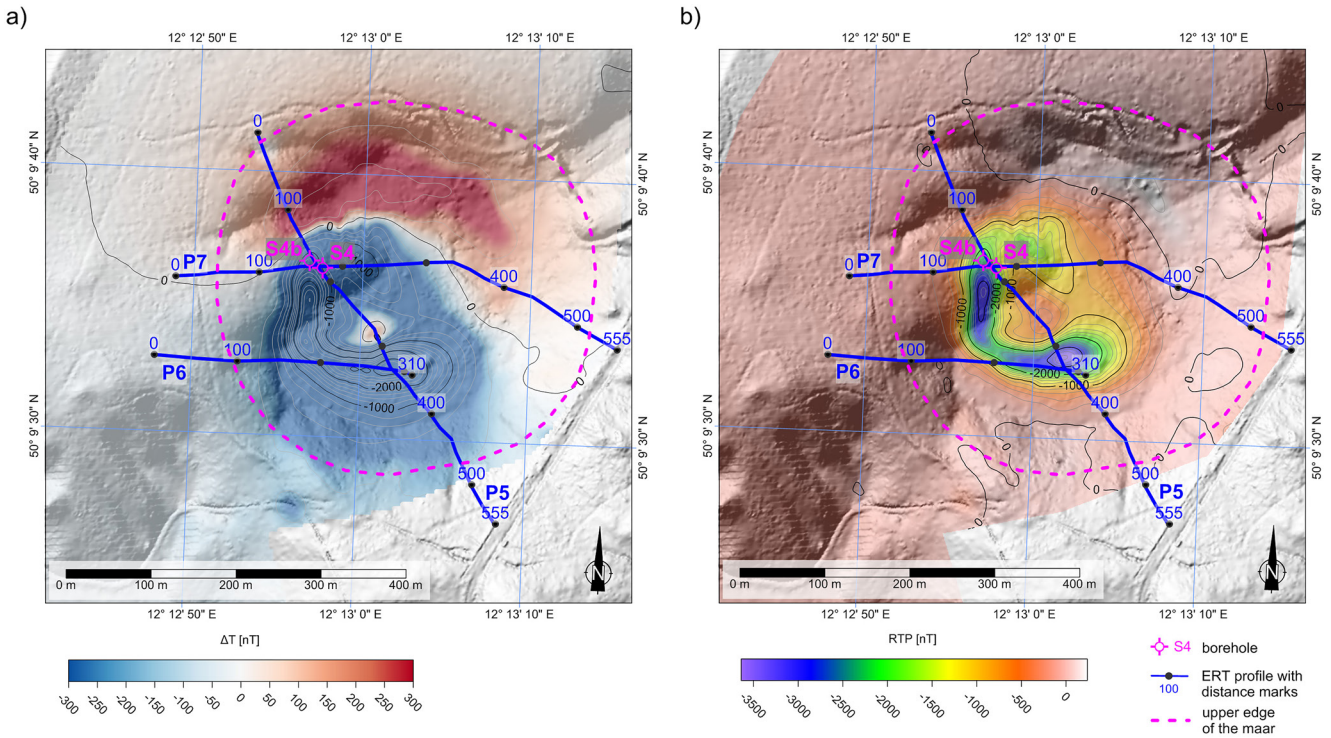

Figure 3. The geomagnetic survey in Bažina maar superimposed on LiDAR-based DEM data. (a) The relative magnetic anomaly ΔT; note its NS-oriented dipole character with a distinct magnetic minimum (blue) in the south and related maximum (red) in the north. (b) The magnetic anomaly reduced to pole (RTP); note its half-circular horseshoe shape with negative values amounting −3,000 nT. The anomaly suggests the presence of a magnetic body with a strong remanent magnetization of reversed polarity. The expected upper edge of the maar is indicated by a violet dashed line. The profiles P5, P6, and P7 for the electric measurements are marked by blue lines; position of both drill holes S4 and S4b are also indicated.

3D mesh consisting of rectangular blocks with the highest resolution of 5 × 5 × 5 m at the surface and slightly decreasing resolution with depth. The inversion and modeling were conducted with the SimPEG python-based software package (Cockett et al., 2015). Low densities of 1.90–2.20 g/cm^3 were attributed to the maar-lake sediments, higher densities of 2.20–2.40 g/cm^3 were assigned to the volcanic breccias (volcanic and country-rock breccias with possible coherent intrusive rocks) below the maar-lake sequences. The granite country rocks with 2.65 g/cm^3 represented the background for modeling of anomalous maar-diatreme gravity. According to numerous studies (e.g., Lorenz & Kurszlaukis, 2007), we applied a funnel shape to model the maar-diatreme geometry, where the slope of the maar-diatreme wall was fitted by curves or lines and tested for the dip angle. Finally, we interpreted the slope of the maar wall by a straight line with a dip of ∼70° from horizontal, which showed a reasonable fit of the observed and calculated gravity.

3.2.2. Magnetic Measurements

The magnetic field measurements were carried out with the portable magnetometer GSM-19GW Overhauser (GEM Systems) with a sampling frequency of 1 Hz and a sensor located 2 m above the ground. The resolution of the instrument is 0.01 nT; the absolute accuracy is ±0.1 nT. The GPS locations were determined by the Garmin GNSS. The variations of the geomagnetic field were determined by the proton-precession magnetometer Satis-Geo PMG-2 with the resolution of 0.1 nT; the normal value of the geomagnetic field at the site during the measurement (June 2019) was based on the World Magnetic Model (Chulliat et al., 2020) and amounted 49,060 nT. Processing of the data involved removal of the outliers (e.g., produced by artificial metallic objects) and corrections for the diurnal variations of the geomagnetic field. In the final step, the data were recalculated by kriging interpolation to a regular grid of 10 × 10 m and plotted as a contour map.

The measured values of the geomagnetic field varied between 44,500 and 49,860 nT. After processing, the relative values ΔT revealed strong magnetic anomaly coinciding with the morphological depression (Figure 3a). This anomaly showed N-S-oriented dipole character with a distinct minimum in the south and related maximum in the north. Because of the dipole character of the magnetic data, these data were reduced to pole (RTP) with the

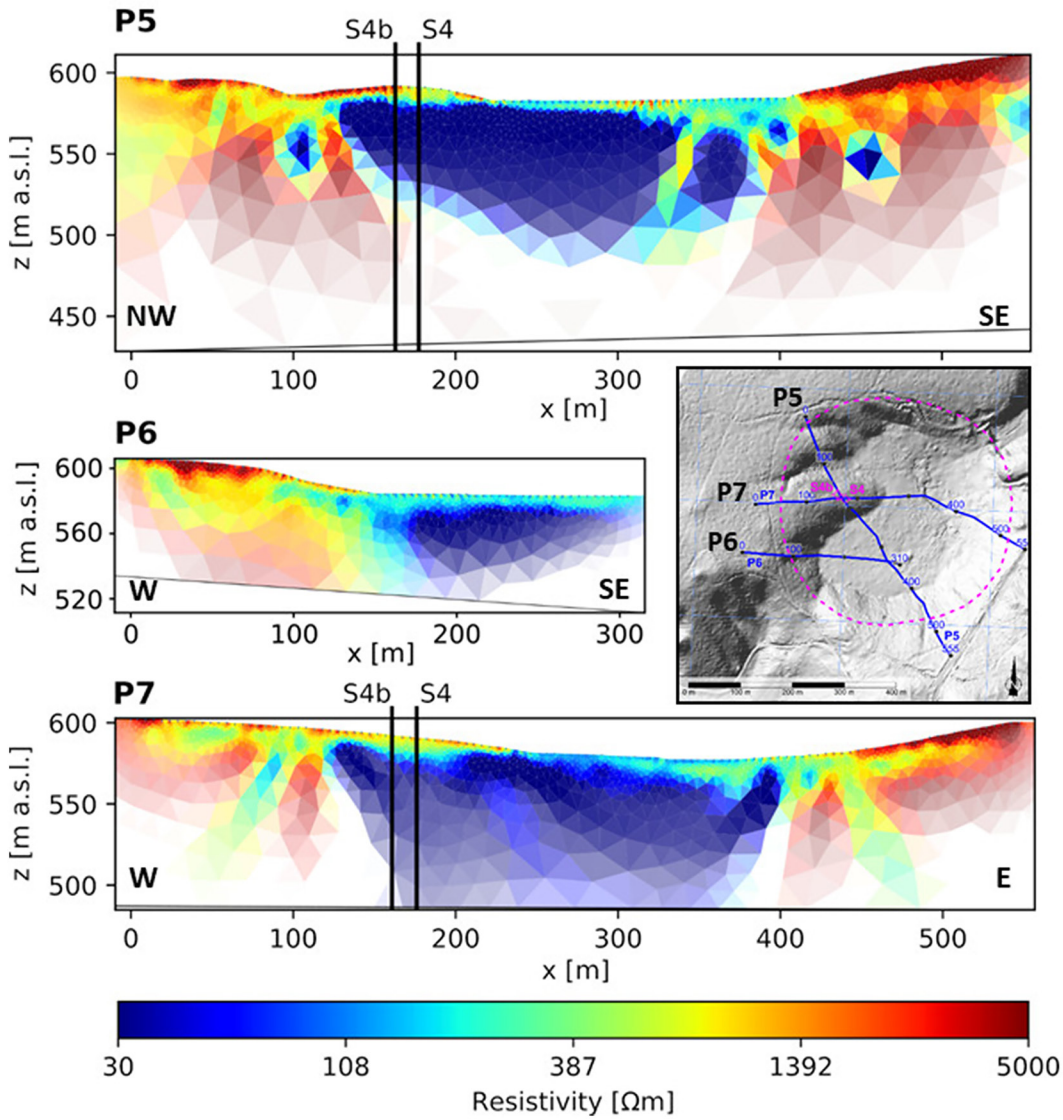

Figure 4. The 2D electric resistivity tomography models along three profiles P5, P6, and P7 depicted in the inset. The color intensity expresses the reliability of resistivity determination. Note low resistivity values (<200 Ωm, blue colors) concentrated in the center of the maar and forming low-resistivity anomaly of a circular shape with very steep edges (~60° from horizontal). The position of drill holes S4 and S4b indicated.

algorithm described by Cooper and Cowan (2005), which enabled to highlight the shape of the anomaly. The RTP results revealed distinct negative values roughly marked by the −1,000 nT contour line and showed the lowest values of more than 3,000 nT below the normal geomagnetic field (Figure 3b).

This negative RTP anomaly was of a half-circular horseshoe shape and its minimum coincided with the southern and western margins of the morphological depression near the expected edge of the diatreme (Figure 3b). Such a setting suggested the presence of a magnetic body with a strong remanent magnetization. Moreover, the magnetic anomaly had the maximum in the north and the minimum in the south (Figure 3a), and the distinct RTP anomaly was negative (Figure 3b), which evinces the reversed polarity of the remanent magnetization. Such a reverse magnetization helped in dating the maar evolution and is discussed later in the text.

3.2.3. Electrical Resistivity Tomography

In addition to gravity and magnetic measurements, a ground resistivity investigation was performed in order to specify spatial distribution of the anomalous bodies and namely their depth. We designed three profiles P5, P6,

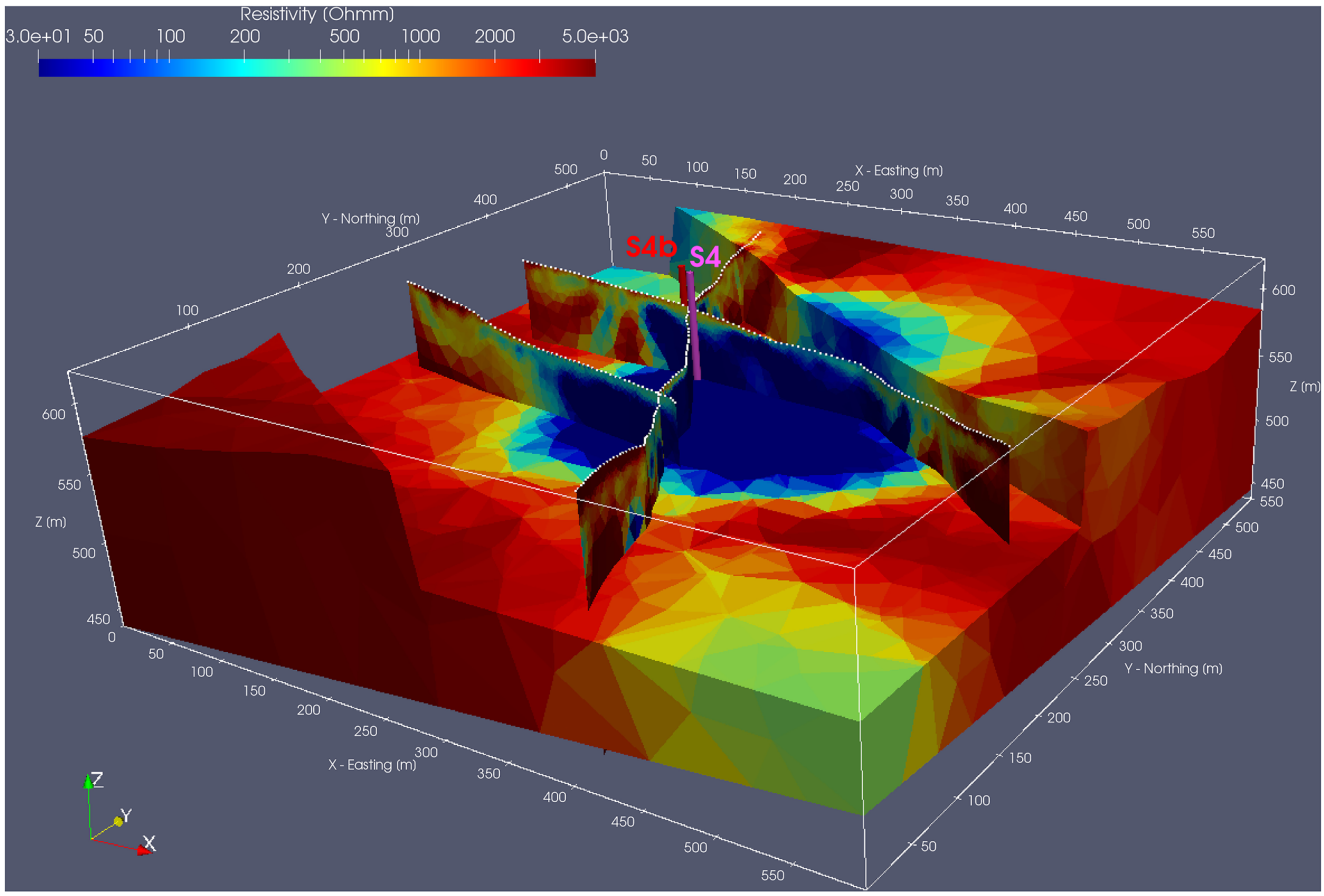

Figure 5. The 3D resistivity model based on all available ERT data (BERT software; Günther et al., 2006). Note low-resistivity anomaly (resistivities <200 Ωm, blue color) of a circular shape. Individual profiles P5, P6, and P7, with boreholes S4 and S4b are highlighted.

and P7 (Figure 4) and carried out field electrical measurements with the ARES II instrument (Gf-Instruments, Ltd.), which included a powerful transmitter (850 W, necessary for measuring large depths and distances) and stainless-steel electrodes. We applied several electrode configurations along the profiles: the Wenner-Schlumberger and dipole-dipole configurations were used at all profiles; the profile P5 was also measured with the pole-dipole and reversed pole-dipole arrays to increase the depth penetration. The inter-electrode distance on all profiles was 5 m. The "infinity" electrode consisted of an array of three 0.75-m-long electrodes grounded in the marsh of the nearby brook, with a distance of ~2,500 m in the direction perpendicular to the P5 profile.

To increase the reliability and resolution in the final inversion, we combined the individual data sets from different resistivity methods, removed the outliers and added the topographical information. For the inversion, we used the BERT software package (Günther et al., 2006; Rücker et al., 2006) and weighted data residuals with the L_1 norm to further decrease the effect of possible measurement errors. The inversion resulted in the electric resistivity tomgraphy (ERT) model along P5–P7 profiles (Figure 4) with the resistivities depicted as triangles of the inversion finite element mesh colored according to model resistivities. In addition, a 3D inversion (using all measured data) with the same inversion software was performed. Although the data coverage was quite low for a detailed 3D model, it was possible to obtain a smooth 3D distribution of resistivities and get a general 3D overview of the investigated structure (Figure 5).

The modeled resistivities ranged between 30 and 5,000 Ωm with strikingly low values confined to the center of the morphological depression (Figure 4). This low-resistivity anomaly (resistivities <200 Ωm) had a circular shape with ~300 m in diameter and exhibited a thickness of ~90–100 m with very steep edges (~60° from horizontal). The near-surface values of resistivities were generally high (300 Ωm and more, often exceeding 2,000 Ωm); however, the surface layer was generally thin, only few meters thick, slightly increasing to ~10 m on the western part of profiles P5–P7. The country rocks at the margins of all profiles exhibited high resistivity zones

Figure 6. The S4b drill core (granite) at the depth of 140.5 m. It shows the maar-diatreme contact with the granites along a sharp plane dipping 68° from horizontal (measured by clinometer) distinctly visible on the granitic core sample.

sometimes exceeding 5,000 Ωm. The transition to the central low-resistivity anomaly was generally sharp; however, it consisted of a number of small-scale low-resistivity anomalies (~100 Ωm and less), especially on profiles P5 and P7, suggesting a more complex geology than just a simple contact of the maar filling sequences with the country rocks.

3.3. Drilling Investigation

3.3.1. Site Selection

The results of geophysical investigations of the circular morphological depression Bažina indicated a structure with circular negative gravity anomaly (Figure 2), horseshoe-shaped negative magnetic anomaly (Figure 3), and funnel-shaped low-resistivity anomaly (Figures 4 and 5). All these results pointed to a volcanic maar origin of the newly discovered structure. To confirm its volcanic origin and explore the maar-diatreme in more detail, a 400 m deep borehole was designed. Moreover, the ultimate target of the borehole was to provide a place for the deployment of a borehole seismometer in the frame of the ICDP Eger project (Fischer et al., 2022). To fulfill such different multidisciplinary targets, the borehole location had to meet several criteria, sometimes with competing objectives. The location was required to be:

1. not far from the maar edge, which would allow to *reach the contact of the maar-diatreme with the country rocks* at a reasonable depth and continue drilling to *deploy the seismic sensor deeply in the solid granitic rocks*;
2. close to the center of the maar, where sediments are less disturbed to *obtain a complete sedimentary record of the maar filling*;
3. in the strong horseshoe-shaped *magnetic anomaly* to reveal its *source*;
4. upon the *elevation* inside the maar near its western edge to *reveal the origin of the elevation*;
5. in only few *accessible parts of the mostly swampy maar.*

Furthermore, the estimated dip angle of the maar walls remained crucial in the decision on the borehole location and limited the selection. The gravity (Figure 2d) and resistivity (Figures 4 and 5) models indicated steep slope of the maar walls (60°–70° from horizontal), which constrained the selection. On the other hand, the magnetic anomaly predisposed the drill site location to the southern or western margin of the morphological depression, the maar.

Based on the evaluation of these aspects, the S4 drilling site was selected optimally to meet most of the above-mentioned criteria. It was located in the western part of the maar, in the area of a small elevation within the maar structure (Figure 1). The elevation provided solid basement for the drilling rig (5) and could answer the questions on the origin of the elevation (4). It coincided with the western place of the horseshoe-shaped negative magnetic anomaly, which could provide direct evidence of its origin (3). Its position at about 140 m from the maar edge with the estimated dip of the maar wall (60°–70° from horizontal) could enable to reach the surrounding granites in ~100–200 m depth, reasonably enough to drill another 200–300 m in the solid granitic rocks for a safe deployment of a seismic sensor (1). Reaching the contact with the granites could also enable to explore the maar-diatreme/granite contact zone, its geometry, and the rate of rock deformation.

3.3.2. Drilling Results

The borehole S4 was realized at the pre-selected site and reached the depth of 400 m. It was designed as vertical, and its inclination did not exceed 2°. The borehole penetrated various volcanic rocks and volcaniclastic deposits in the fill of the Bažina maar crater. Then, it reached the granitic country rocks (Figure 6) at the depth of 170 m, from where it continued down to 400 m through the solid granites. These granites were of two types, less-altered and strongly altered biotitic granite, porphyritic with alternating coarse and fine-grained varieties (for details on granites, see Fischer et al., 2022).

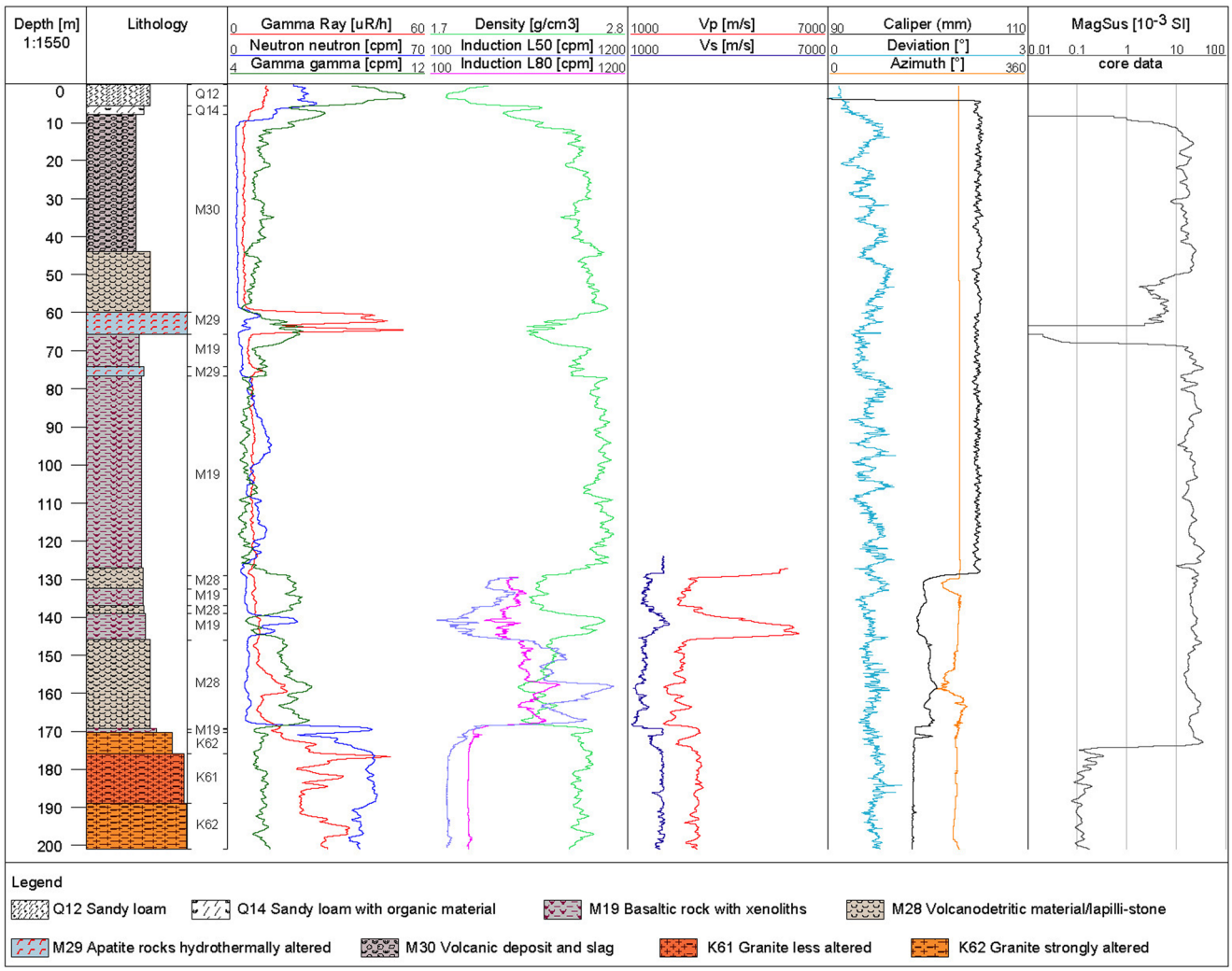

Figure 7. The lithology profile and logging data of the S4 borehole in the depth range of 0–200 m. The missing data (*Vp*, *Vs* and inductions) in a depth range of 0–130 m are due to provisional casing supporting the borehole.

The coherent volcanic rocks and volcaniclastic deposits of the S4 borehole (Figure 7) comprised almost the whole sequence of the Bažina maar-diatreme filling, except for few upper meters of the Quaternary colluvial deposits. These sequences started with the 36-m-thick volcaniclastic deposits at depths of 7.8–43.7 m and were followed by basaltic scoria lapilli-stones (depths of 43.7–60.0 m). The upper volcanic sequences were interrupted by a 6-m-thick vein of apatite rock (depths of 60–66 m) intersecting the volcanic layers. At the depth of 66 m, the S4 drill hole reached solid basaltic lava, which extended to the depth of 129.4 m (range of 66.6–129.4 m). The resting sequence until the 170 m depth (range of 129.4–170.0 m) represented the pyroclastic rocks and lavas (olivine melilitite). In such a way, the apatite rock intruded along the contact between the upper scoria deposits and the olivine nephelinite underneath. Moreover, the olivine nephelinite intruded into the sequence of pyroclastic rocks and lavas (olivine melilitite), preserved underneath this intrusion until the contact with the granitic country rocks.

The S4 drill core revealed a complex lithology of volcaniclastic rocks and olivine nephelinite feeding conduit interrupted by the apatite rock. This invoked questions about the lateral extent of these units and the size of the feeding conduit. With the aim to get the answers to these problems and to confirm the dip angle of the maar wall, a parallel S4b borehole was designed. It was drilled 15 m apart from the S4 drill hole toward NW, a bit closer to the maar edge (Figure 1). This S4b borehole (also vertical) penetrated similarly the volcanic rocks and volcaniclastic deposits of the maar fill. Finally, it reached the contact with the granites at the depth of 140.5 m (Figure 6) and terminated in granites at the depth of 150 m (Figure 8). However, though close to the S4 hole, the S4b borehole did not cut the apatite rock.

10.1029/2023EA003009

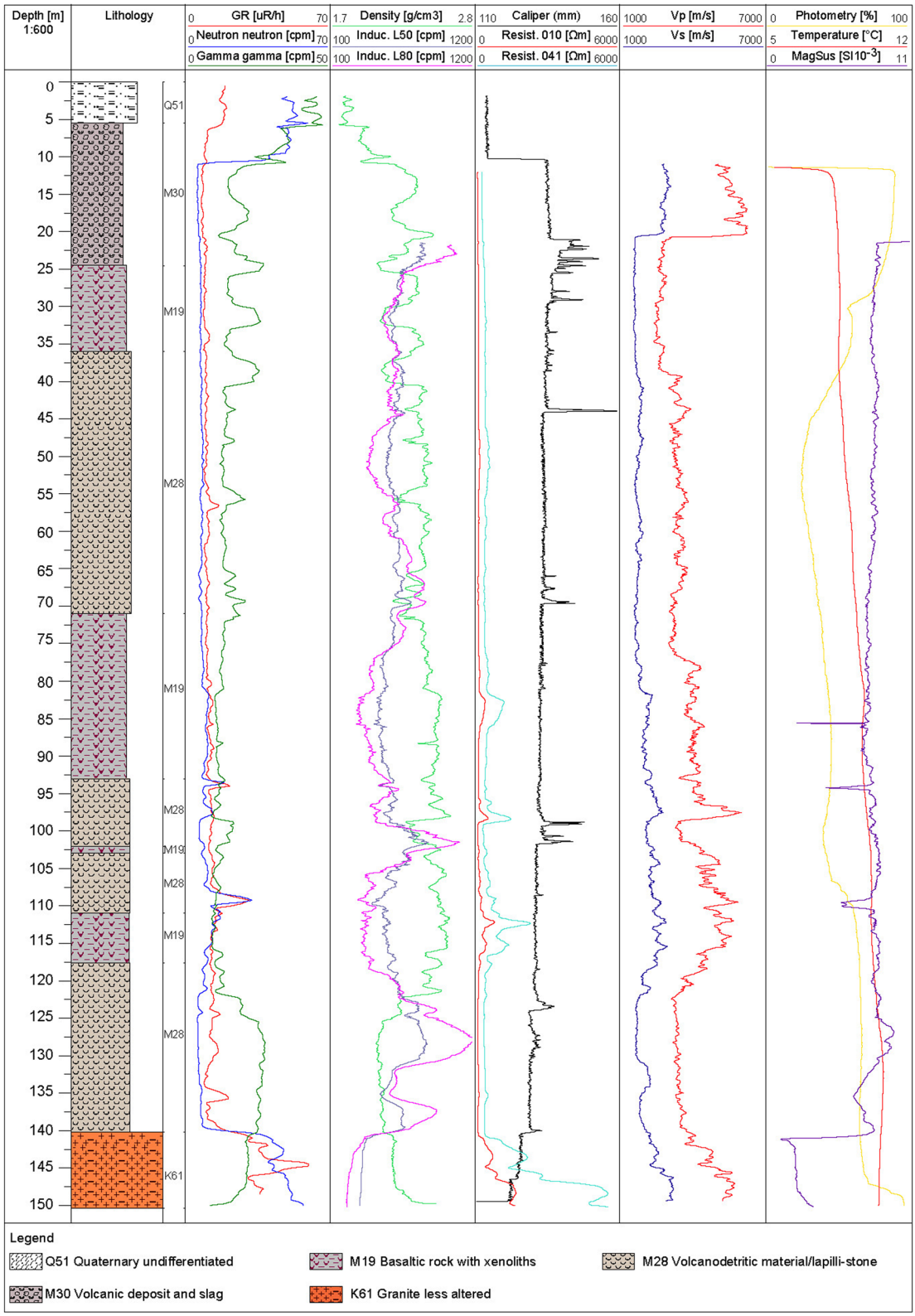

Figure 8. The lithology profile and logging data of the S4b borehole. GR - gamma ray.

As revealed by both S4 and S4b cores, the contact with the granites was sharp, along a plane dipping 68° from horizontal (Figure 6). Another independent estimate on the slope of the diatreme wall resulted from the spatial locations of both boreholes and their contacts with granite at depth and amounted 68° (lower estimate resulting from non-radial two borehole locations within the maar). These findings agreed well with the results from the pre-site geophysical investigation predicting the dip of 70° from the gravity modeling and 60° from the ERT results. The granite was strongly altered at a place of S4 (at a depth of 170 m), while less altered at a place of S4b (at a depth of 140.5 m); in both cases, the granite was porphyritic, biotitic and coarse-grained, with numerous inclined fractures supporting the concept of an abrupt maar-forming phreatomagmatic explosion. Detailed petrographic description of the main volcanic lithologies along the S4 and S4b boreholes is presented in the Supplementary Information (SI).

The results from drillings of both boreholes gave the answer to two principal questions: (a) The volcaniclastic deposits together with the underlying olivine nephelinite and olivine melilitite (basaltic *s.l.*) lavas represent the source of the magnetic anomaly. (b) The near-surface elevation is composed of colluvium and volcaniclastic deposits suggesting its origin from volcanic activity following the maar-forming eruption.

3.3.3. Well-Logging and Core Measurement

The well-logging data provided further constrains on stratigraphy of both S4 and S4b boreholes. Since we focused on the maar-diatreme structure and the S4 borehole reached the granitic country rocks at the depth of 170 m, we focus on the depth range of 0–200 m along the S4 borehole profile (Figure 7); the S4b profile is presented for the complete drilled depth range of 0–150 m (Figure 8). The well-logging comprised gamma ray, neutron-neutron, density, resistivity, *P* and *S* wave velocity, focus electrical resistivity, electrical conductivity, caliper, and temperature measurements. All logging measurements were depth matched using the gamma ray as the reference logging present in all probes (Fischer et al., 2022).

The variation in lithology within the maar-diatreme structure was well captured by the gamma ray log. This applies especially for the S4 borehole, where the natural gamma ray log shows very low average values with a sharp spike of 50 μR/h for the apatite rock, clearly delimiting this formation at depths of 60–66 m. Similarly, the onsets of granitic rocks at 170 m (S4) and 140.5 m (S4b) with increase values are clearly visible from an abrupt increase of natural gamma ray logs related to the higher content of the radioisotopes in granite. Interestingly, also neutron-neutron log clearly delimits the underlying granites by the increase of slow neutron count due to smaller porosity of the granites compared to the overlying volcaniclastic deposits.

The magnetic susceptibility measurements complemented the logging and supported the resulting lithologies. In case of the S4b borehole, the magnetic susceptibility was measured during logging (Figure 8); in case of the S4 borehole, the magnetic susceptibility was obtained from the core samples (Figure 7). In the latter case, the measurement was realized by portable hand-held kappameter KT-5, consistently probing all core samples at the same angle. Since some pieces of the core were detritic, the susceptibility values were approximated and have to be considered as relative. The observed values ranged from less than 0.01×10^{-3} u.SI for near-surface sediments and some parts of granite and apatite rocks, to about 40×10^{-3} u.SI for volcanic and volcaniclastic rocks (Figures 7 and 8). These increased values reflecting coherent volcanic rocks and volcaniclastic deposits clearly delimited the contact with granites. The variability in lithology between two sub-parallel boreholes S4 and S4b (Figures 7 and 8), which are only 15 m apart, is remarkable, and demonstrates the heterogeneity close to the maar-diatreme edge.

4. Discussion

4.1. Evaluation of Combined Geophysical and Drilling Results

Combination of different geophysical results constrained by the S4 and S4b lithological profiles enabled more profound geological interpretation and overcame some of the limitations of individual geophysical methods. In case of the electrical methods, the limitations relate to the depth of investigation and the fact that similar resistivities can represent different rocks. This is documented in Figure 9, which matches the ERT cross-section along the P5 profile with lithological profiles of both boreholes. According to resistivities, the ERT section can be divided into three domains: the central domain with low resistivities in its upper part (corresponding to the maar-fill sequences) and two high-resistivity domains on both sides of the profile (corresponding to granite country rocks).

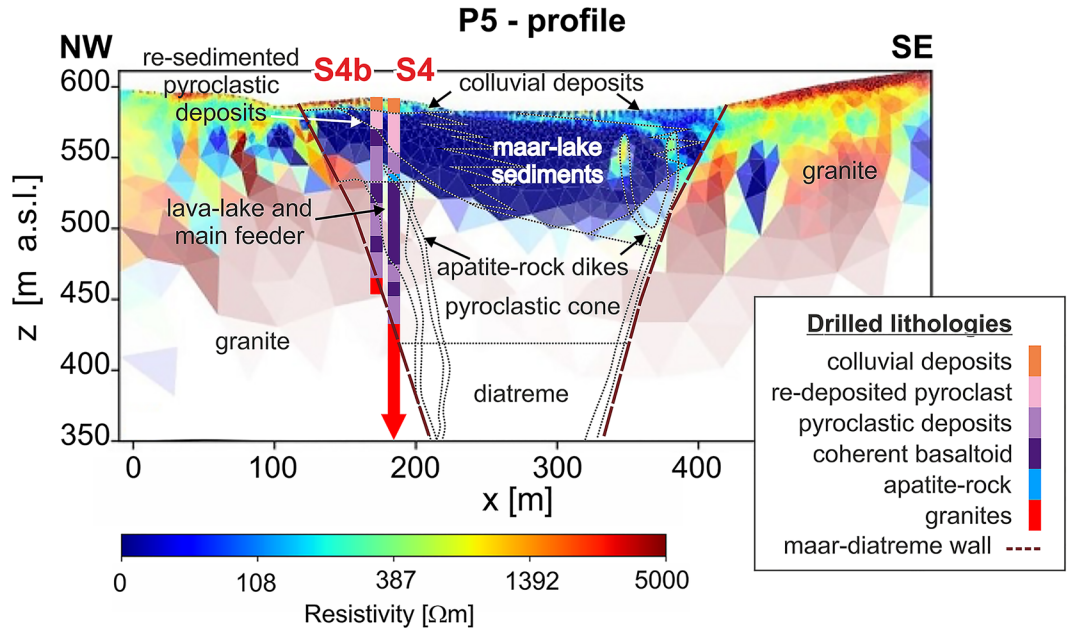

Figure 9. The interpretation of the electrical resistivity tomography (ERT) cross-section along P5 profile together with lithologies from the S4 and S4b boreholes. The color intensity expresses the reliability of the ERT resistivity determination and its decrease with depth. Note its faster decrease in the central low-resistivity domain (maar-lake sediments) compared to the outside high-resistivity domains (granites).

The color intensity expresses the reliability of the resistivity determination and decreases with depth. Moreover, the color intensity decreases faster in central low-resistivity domain than outside in high-resistivity domains. This is caused by focusing of the electric current in the conductive layers, which is an inherent characteristic of the electrical resistivity methods. As a result, the ERT does not provide information on the resistivity distribution of the maar-filling sequences beneath the 90 m depth.

The comparison of the ERT with the lithological profiles shows that the low-resistivity domain (~100 Ωm and less) corresponds to the altered and water-saturated pyroclastic deposits, which can be both primary and re-sedimented. Similar resistivities extend to the SE to the depths of 90–100 m and fill the remaining part of the maar; however, their origin may be different. In the central and SE parts, these low-resistivities may rather represent the maar-lake sediments and the similarity in resistivity values is evoked by porosity and water saturation, a sensitive factor in the electrical methods (e.g., Soleymanzadeh et al., 2021).

The increased resistivities (~200 Ωm, light blue color) below 60 m depth at the place of both boreholes correspond to the coherent rocks and include the apatite rock and the olivine nephelinite. With increasing depth, the resistivities increase and reach high resistivities at depths of 70 m (S4b) and 100 m (S4) similar to resistivities for the country rocks (>1,500 Ωm, reddish color). Though these high resistivities (at depths of 70–140 m for S4b and 100–170 m for S4) are similar to resistivities of the granite country rocks, they do not represent granite, but they represent solid volcanic rocks within the maar-diatreme.

This makes the low-resistivity central domain asymmetric and shallower in the NW (Figure 9) and evokes the impression of the asymmetric shape of the whole maar. However, the drillings revealed that the high-resistivity zone below 40 m depth corresponds to the volcanic feeding conduit that probably evolved along the weakened contact with the maar-diatreme wall. Thus, the true maar-diatreme shape is symmetric. This clearly surpasses the resistivity results especially in case of the intrusions within the maar, where granites (country rocks) and basalts (intrusions) have similar high resistivities and thus are indistinguishable by resistivity methods. The drillings provide direct evidence and restrict from implying false interpretations of the Bažina maar evolution.

Gravity modeling, which suffers from a trade-off between density and size of the modeled body, benefited from the ERT results in estimating the depth of the maar filling (the upper low-density layer with the density of 1.9–2.2 g/cm^3; Figure 2d). It was constrained by the depth of low resistivities above ~100 m and resulted in the

optimal fit between measured and modeled gravity curves. The dip of the maar-diatreme wall was concluded from the gravity model. Its combined interpretation with the ERT model resulted in a robust estimate of the maar-wall dip between 60° and 70° from horizontal. The ERT model also served for the identification of the maar edge at profiles P5 and P7 and allowed for precise location of the borehole. Such a location at ∼140 m from the maar edge with the estimated dip of the maar wall in the range of 60°–70° anticipated to reach the contact of the maar with the surrounding granites in ∼150–200 m depth, reasonably enough to drill another 200–300 m in solid granitic rocks for a safe deployment of the seismic sensor. The measured inclination of the maar-diatreme wall of 68° would suggest the depth of the diatreme at ∼380 m; assuming larger inclination of the maar-diatreme wall at deeper parts concludes its depth at ∼600 m (Figure 10).

The location of the borehole was further constrained by the magnetic field measurements, which revealed pronounced magnetic anomaly indicating presence of a magnetic body with a strong remanent magnetization. The horseshoe shape of this anomaly (Figure 3b) suggests a magma ascent along the diatreme walls (Figure 10). The arrangement of the remnants of pyroclastic cones also supports this model. In addition, the lavas emitted from the individual cones formed rather limited tongues, emphasizing the magnetic anomaly bordering the diatreme rim. In the case of larger lava volume emission, the resulting lava lake would fill the remaining part of the maar-crater depression next to the cones, producing significant, almost isometric, magmatic anomaly in the central to northeastern part of the maar, as documented in other lava-filled maars (e.g., Bolós et al., 2012; Valenta et al., 2014).

The selection of the drilling site on the top of the small elevation of hitherto unknown origin within the maar structure was fortunate. Both S4 and S4b boreholes identified pyroclastic deposits overlying intrusive facies and feeding conduits, suggesting that the elevation represents an erosional remnant of a pyroclastic cone. Moreover, a close-up re-evaluation of the morphological data (LiDAR-based DEM) enabled to detect other small elevations within the depression more to the north (Figure 10a). Being of similar character, these elevations can represent sequential volcanic activities where at least three pyroclastic cones grew within the maar crater. The alternation of pyroclastic deposits (explosive phase of pyroclastic cone growth) with the lava layers (effusive event terminating each explosive event) in the S4b borehole suggests a repeated activity associated with the growth of successive pyroclastic cones inside the maar crater.

4.2. Eruption Styles and Evolution of Two Volcanoes

The S4 and S4b borehole lithologies revealed products of two subsequent volcanic activities within the Bažina maar following the initial maar-forming explosion (Figure 10).

1. The older activity is documented by the hypocrystalline and poorly vesiculated character of the pyroclasts in the lowermost part of the successions (below the olivine nephelinite intrusion), which evidences the hydromagmatic fragmentation (Cole et al., 2001; McPhie et al., 1993; Murtagh & White, 2013). Predominance of juvenile (magmatic) pyroclasts and relatively low content of country rock xenoliths is in a good agreement with the deposits of the Surtseyan style eruption (Kokelaar, 1983; Németh & Kósik, 2020a). Shallow-water hydromagmatic explosion of the Surtseyan style corresponds well with the initial stage of a pyroclastic cone growth within the shallow-water settings (e.g., Gjerløw et al., 2015; Murtagh & White, 2013; Németh et al., 2006; Németh & Kósik, 2020b), in our case the already existing maar lake. The Surtseyan style eruptions were associated with several lava flows, as evidenced from the sequence. Similar successions with lava flows embedded within Surtseyan pyroclastic deposits were documented already during Surtsey eruption (1963–1967; Thordarson & Sigmarsson, 2009), and are also known from ancient volcanic successions (e.g., Martin & Németh, 2004).
   The overlying body of the olivine nephelinite (with almost 63 m of the drill-core sequence) is too thick to represent a lava flow of mafic (low-viscosity) volcanic rock. More likely, this body represents a conduit of the pyroclastic cone. According to the transition to the highly vesicular or even brecciated facies in the uppermost part, the feeding conduit was probably associated with a lava lake within the intra-cone crater. The growth of the pyroclastic cone led to the insulation of the eruption from the lake-water influence, similarly as documented by Németh et al. (2006) in Vanuatu.
2. The subsequent activity (documented by the drill core above 60.0 m depth) is characterized by lower intensity of fragmentation and good vesiculation suggesting rather the Strombolian style eruption (e.g., Kiyosugi et al., 2014; McPhie et al., 1993; Taddeucci et al., 2015). In contrast to weakly vesiculated and more fragmented

10.1029/2023EA003009

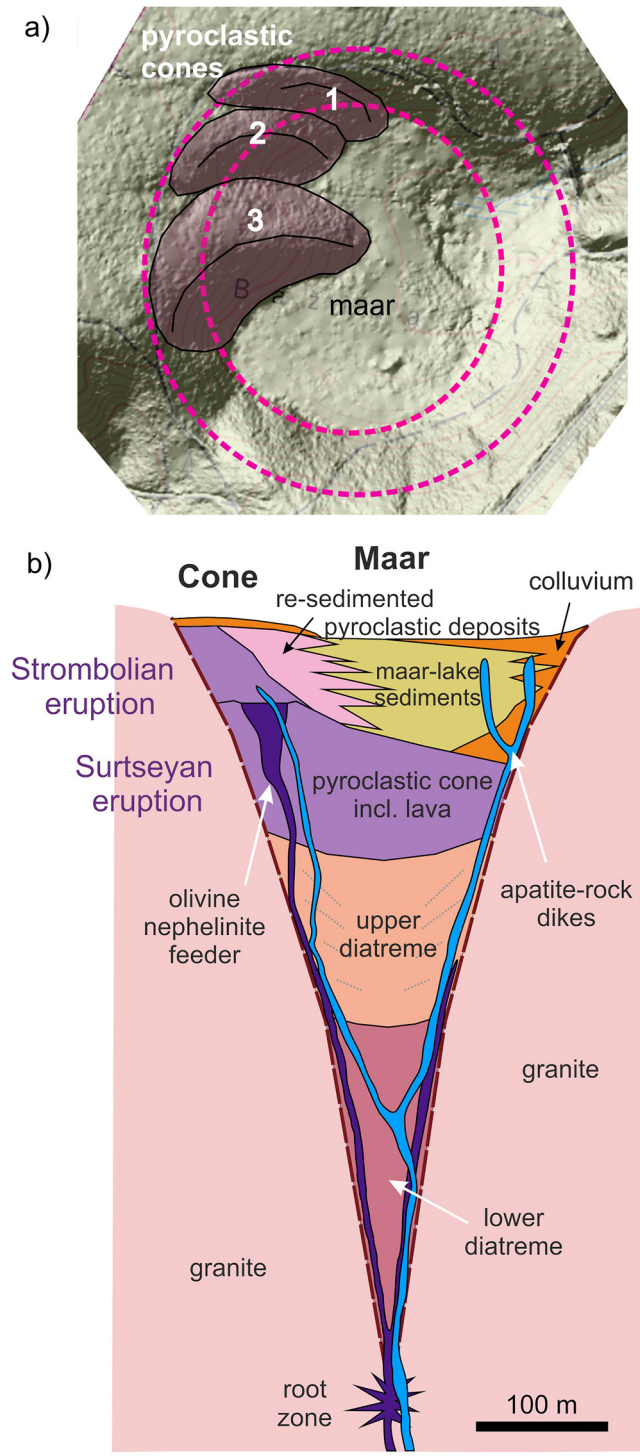

Figure 10. Interpretation of the Bažina maar hosting the post-maar pyroclastic cones: (a) the morphological elevations within the Bažina maar; #1, #2, #3 suggest possible successions of the pyroclastic cones developed in time (#1 being the oldest). Violet dashed lines delimit the maar crater. (b) The schematic Bažina maar-diatreme cross-section based on geophysical and drilling data. Note the older pyroclastic deposits including lavas of the Surtseyan eruption followed by younger pyroclastic deposits with lavas of the Strombolian eruption forming scoria cone detected at the surface. The Strombolian scoria cone grew atop the Surtseyan cone, when the growing cone breached water level of the maar-hosted lake. Redeposition of loose pyroclastic material washed from the Strombolian cone supplied the lacustrine sedimentation. The geometry of the maar-diatreme structure suggests the depth of the diatreme at ~600 m.

Surtseyan lapilli, the highly vesiculated Strombolian scoria fragments evidence drier eruption driven mainly by the expansion of volcanic gasses.

The emplacement of the apatite-rock vein terminated the construction of the post-maar pyroclastic cones, which is evidenced from the scoria impregnation with the apatite (depths of 60–66 m). Porosity with the absence of holocrystalline texture and the apatite crystal tips slicked into the open space suggest crystallization of the apatite from fluids, not from melt, and point to its possible hydrothermal origin.

Significant part of the emerged scoria cone was subject to erosion and re-deposition, evidenced by the S4 drill core at 7.8–43.7 m depths. However, limited space of the maar lake, moreover within the maar-hosted pyroclastic cone, did not allow many re-depositional processes. The massive matrix-supported beds can be attributed to gravitational slumps of partly altered (argillized) pyroclastic deposits. The layered domains seem to result from rain-wash of the loose pyroclastic material, which is supported by the origin of quartz-rich beds. The quartz-rich beds might evoke a renewed explosive activity deeper in the diatreme with high amount of country rock granite; however, such a type of eruption would blow up the existing pyroclastic cone and thus this scenario is rather unlikely, as the pyroclastic cone is well preserved. On the other hand, a tephra-ring (not preserved at present) formed during the maar eruption had to be dominated by country rock fragments (Lorenz & Kurszlaukis, 2007). These granite-derived pyroclasts from the tephra-ring could be washed down to the maar crater and support the quartz admixture in the layered domains much better.

To conclude, the combination of the drill-core and geophysical data enabled to construct the Bažina volcano model and decipher the eruption history (Figure 10b). The funnel-shaped crater formed by the maar-diatreme eruption hosted subsequent volcanic activity. This phase had Surtseyan style character (characterized by shallow-water interactions between water and lava) due to hydrovolcanic eruptions within the lake occupying the maar crater. When the growing edifice of the Surtseyan tuff cone breached the water level, the eruption style shifted to Strombolian (drier eruption), forming a scoria cone capping the earlier tuff cone edifice. The process of the growing cone breaching the water level might be facilitated by water loss due to its consumption in hydrovolcanism. Later, the lake could re-establish to create an environment where re-mobilized pyroclastic deposits of the intra-maar volcano could sediment.

4.3. Age Determination

The Bažina maar-diatreme volcano belongs to the Cenozoic alkaline intraplate volcanism related to the opening of the CDG (Ulrych et al., 2011) and it is one of the maars associated with the TF delimiting the CDG from the west. Nowadays, it does not host any lake, probably because of the crater filled with sediments, possibly also associated with draining of the crater through its breached edge in NW (where the maar opens to a small brook). The same applies to its twin maar Ztracený rybník and the two other maars further to the south, the Mýtina and Neualbenreuth maars.

The age of the Mýtina and Neualbenreuth maars are determined from Ar-Ar geochronology at 0.27–0.29 Ma, dating them to the Mid Pleistocene (Mrlina et al., 2009; Rohrmüller et al., 2018). Apart from the maars, the area also hosts two Quaternary scoria cones, Komorní hůrka (KH) and Železná hůrka (ZH), one of the youngest Quaternary volcanoes on the territory of the Czech Republic (Figure 1). These volcanoes are of the Strombolian type with olivine nephelinite lava flows and pyroclastic deposits and their estimated age is 0.15–0.40 Ma.

The age of the Bažina maar has not been dated yet, but even without geochronological data, the reverse polarity of the magnetic anomaly identified from the magnetic investigation can provide some estimates on the age of the eruption. The pronounced Bažina magnetic anomaly suggests the presence of a magnetic body with a strong remanent magnetization. Moreover, its negative character evinces reversed polarity of the magnetization. As the last geomagnetic reverse period (Brunhes-Matuyama) terminated 0.78 Ma ago, the eruption and crystallization of the lava cannot be younger than this age. This agrees with the fact, that smaller but positive magnetic anomaly detected in the Mýtina maar (Mrlina et al., 2009) suggests the eruption of Mýtina during the normal geomagnetic field, that is, in the time span between 0 and 0.78 Ma. The Ar-Ar age determination (groundmass) of the Mýtina maar yields 0.29 Ma (Mrlina et al., 2007), which clearly fits these implications. Moreover, comparing the age of all volcanoes along the TF, we can infer that the eruption of the Bažina maar documents the oldest (maybe opening) phase of the Pleistocene volcanic activity in the area.

The Plio-Pleistocene volcanism of the Bohemian Massif represents the reactivation of NW-SE trending strike-slip tectonics (Rajchl et al., 2009); however, the individual areas across the Bohemian Massif did not experience volcanic activity simultaneously. Thus, the Bažina maar age of more than 0.78 Ma extends the volcanic

activity associated with the TF further to geological past and provides another evidence into the mosaic of the post-Miocene evolution of central Europe.

4.4. Magmatism and Tectonic Context

The erupted rocks of the Bažina maar are compositionally similar to olivine nephelinite and olivine melilitite lavas and juvenile bombs erupted from nearby KH and ZH scoria cones and other Pleistocene volcanic rocks along the TF (Ulrych et al., 2013). Such ultrabasic magmas result from a very low-degree partial melting of the asthenospheric mantle and suggest the ascent of small portions of magma directly to the surface without resting in any magmatic reservoir. This is supported by the results of Plomerová et al. (2016), who discussed the source of hot magma material in the lithospheric mantle at ∼80–170 km depths and its ascent along boundaries of lithosphere mantle domains in the West Bohemian triple junction (Babuška et al., 2007). However, unlike the other maars associated with the TF, the magma supply of the Bažina maar continued after the initial maar-forming eruption and gave the rise to a set of pyroclastic cones inside the maar.

The continuation of a magma supply persisting after the maar eruption and leading to a formation of a scoria cone is also observed in some other maars around the world. Amin and Valentine (2017) detected a scoria cone at the maar edge; other scoriae within the crater were identified by Németh et al. (2008, 2012), Ross et al. (2011), Swanson (1989), or Güllü and Kadıoğlu (2019). However, the pyroclastic deposits produced by the eruptions after the Bažina maar-forming eruption are characterized by higher fragmentation degree, low vesiculation, and pyroclasts with glassy (palagonite) groundmass suggesting hydrovolcanic eruptions in maar-hosted lake. The upper layers differ in coarser grain-size (lower fragmentation degree) and higher vesiculation and imply that the lake water had smaller influence on the growing pyroclastic cone.

From a general point of view, the Pleistocene volcanoes in West Bohemia are aligned along the TF, the whole-crustal feature (Hrubcová et al., 2017) delimiting the Cheb Basin in the west. The age determination of the individual volcanoes within this volcanic field points to the active volcanism in the time span of at least 0.5 Ma with the activity probably initiating in the north and propagating to the south. While the size of this volcanic field is small (∼25 km) with only 6–7 constructs, the evolution time span is huge (>0.5 Ma) and points to the persistent long-lasting activity; however, with extremely low magma productivity. Compared to numerous volcanoes in other Cenozoic volcanic fields (e.g., Petronis et al., 2013; Sirocko et al., 2013), the number of volcanic edifices in West Bohemia is small.

5. Conclusions

We inspected the maar-diatreme volcano with scoria pyroclastic cones inside. Such a volcanic structure was revealed from multidisciplinary geophysical and drilling investigations carried out in the Pleistocene Bažina maar in the western Eger Rift (Czech Republic) near Germany. The detection of the maar initiated with the evaluation of the morphological (LiDAR-based DEM) data. The existence of the maar-diatreme structure was confirmed by circular negative gravity anomaly, funnel-shape low-resistivity anomaly, and strong magnetic anomaly. The gravity modeling estimated the dip of the maar-diatreme wall, magnetic anomaly suggested the presence of a magnetic body with a strong remanent magnetization and reversed polarity, the ERT model specified the spatial distribution of the maar fill, its depth, and estimated the inclination of the maar-diatreme wall. Knowledge of the structure from multidisciplinary geophysical measurements enabled to locate optimally two boreholes (S4 and S4b) within the maar crater. Different geophysical models constrained by lithological profiles enabled more profound geological interpretation and overcame some of the limitations of individual geophysical methods.

Two vertical boreholes (S4, 400 m and S4b, 150 m) were located on a small elevation within the maar crater. They penetrated volcanic rocks and volcaniclastic deposits with the olivine nephelinite feeding conduit that represents significant part of the drill cores. The elevation turned out to be the remnant of a pyroclastic cone inside the maar, formed by several later eruptions. The contact of the maar with the granite country rocks was sharp, along a plane dipping ∼68° from the horizontal. It was in agreement with the results from the pre-drill geophysical investigations and with the inclination deduced from the spatial locations of two drilled granite (country rock) contacts at depths. The granite, sampled by the drilling, showed numerous inclined fractures supporting the concept of country-rock shattering as a result of an abrupt phreatomagmatic explosion. The geometry of the maar-diatreme structure suggests the depth of the diatreme at ∼600 m.

The eruptive history of the Bažina maar revealed several stages of volcanisms with different eruption styles. The activity initiated with phreatomagmatic maar explosion. It was followed by the Surtseyan style tuff cone formation, which gradually grew until it breached the maar lake level. Consequently, the eruption shifted to the Strombolian style, building a capping scoria cone. In the meantime, the maar lake diminished supplying the Surtseyan explosions. In the last stages, the altered and eroded pyroclastic deposits of gradually eroded intra-maar volcano(s) were collected in the lake, which again established within the maar crater. Lately, the apatite rock intruded along the contact between the upper volcaniclastic scoria deposits and the olivine nephelinite underneath. This apatite rock represents unusual rock-type with hydrothermal origin, and its further investigation will help to understand the volcanic and fluid-flow regimes of West Bohemia.

The age of the Bažina maar eruption estimated from the reverse polarity of the detected magnetic anomaly implies that the effusion and solidification of the lava during the eruption must be older than 0.78 Ma (Pleistocene). Comparing the age of all volcanoes along the TF shows that the Bažina maar belongs to the oldest (maybe opening) phase of the Pleistocene activity in this area. Results from the planned radiometric dating will reveal more precise age determination as well as the time evolution of this two-stage volcanic episode. Nevertheless, disregard the precise dating, the active volcanism in West Bohemia span at least 0.5 Ma and propagate along the TF. This volcanic field is relatively small (~25 km) with only 6–7 volcanoes; however, the eruptive history spans a long-term period (more than 0.5 Ma).

To conclude, our results show how the optimal combination of different geophysical methods led to a successful location of the exploration boreholes and enabled to complement geophysical results with borehole lithologies and well-logging interpretations. This revealed a unique structure of the maar volcano with several generations of eruptions. Our approach clearly proved the benefit of a multidisciplinary methodology, where otherwise a sole application of purely one approach (either geophysical or geological) would provide only partial and possibly misleading results.

Details of the internal structure of the maar hosting a pyroclastic scoria cone improve our understanding of volcanic processes and tectonic evolution at the western margin of the Eger Rift. To facilitate its understanding, the simplified evolution of the Bažina maar volcano is visualized following the principles for 3D geological animations after Rapprich et al. (2017), and it is accessible at https://www.youtube.com/watch?v=VxhFrM6WR8c.

Data Availability Statement

Data for the paper are freely available at Zenodo repository (Hrubcová et al., 2023, https://doi.org/10.5281/zenodo.7889693); for data description see README.txt file in this repository. The repository contains all geophysical data, that is, the ground resistivity, gravity and magnetic measurements, together with the lithology and logging data. The LiDAR-based DEM (DMR 5G) data used for detection and visualization (Figures 1, 3, 4, and 10) in QGIS (Free and Open Source Geographic Information System) were provided from the State Administration of Land Surveying and Cadastre of the Czech Republic (https://geoportal.cuzk.cz; last accessed 23/9/2022). The SRTM elevation data for gravity measurements and visualization (Figure 2) were provided from the USGS (https://www.usgs.gov/centers/eros/science/usgs-eros-archive-digital-elevation-shuttle-radar-topography-mission-srtm-1; last accessed 09/2022) and plotted with the Golden Software Surfer program (https://www.goldensoftware.com/products/surfer). The magnetic data (Figure 3) were processed and plotted as a contour map using algorithms available from the Golden Software Surfer program (https://www.goldensoftware.com/products/surfer). The 2D and 3D resistivity models (Figures 4, 5, and 9) were created with the open source BERT (Boundless Electrical Resistivity Tomography) software (Günther et al., 2006). The evolution of the Bažina maar volcano was visualized following the principles for 3D geological animations (Rapprich et al., 2017); the animation is accessible at https://www.youtube.com/watch?v=VxhFrM6WR8c.

Acknowledgments
The drillings of S4 and S4b were funded by the ICDP-Eger Rift project of the International Continental Drilling Program (ICDP), German Science Foundation (DFG), GFZ Potsdam and large project of the Czech infrastructure CzechGeo (CZ.02.1.01/0.0/0.0/16_013/0001800) and CzechGeo/EPOS (LM2015079). The work of T. Fischer and J. Vlček was supproted by Czech Science Foundation (23-07490K). We thank the team of drillers from Geoněmec - vrty, s.r.o., with special thanks to František Kalenda and Milan Němec. We also thank Simona Pierdominici for plotting the well logs. Petrography of volcanic rocks was funded by the Strategic Research Plan of the Czech Geological Survey (DKRVO/ČGS, 2018–2024). We are grateful to Károly Németh for detailed comments and suggestions that helped to improve the manuscript. We also thank the editor (Helen Glaves) and the reviewer (Marco Neri) for their help in improving the manuscript.

References

Amin, J., & Valentine, G. A. (2017). Compound maar crater and co-eruptive scoria cone in the Lunar Crater Volcanic Field (Nevada, USA). *Journal of Volcanology and Geothermal Research*, *339*, 41–51. https://doi.org/10.1016/j.jvolgeores.2017.05.002

Babuška, V., Fiala, J., & Plomerová, J. (2010). Bottom to top lithosphere structure and evolution of western Eger Rift (central Europe). *International Journal of Earth Sciences*, *99*(4), 891–907. https://doi.org/10.1007/s00531-009-0434-4

Babuška, V., & Plomerová, J. (2001). Subcrustal lithosphere around the Saxothuringian-Moldanubian suture zone—A model derived from anisotropy of seismic wave velocities. *Tectonophysics*, *332*(1–2), 185–199. https://doi.org/10.1016/s0040-1951(00)00255-9

Babuška, V., Plomerová, J., & Fischer, T. (2007). Intraplate seismicity in the western Bohemian Massif (central Europe): A possible correlation with a paleoplate junction. *Journal of Geodynamics*, *44*(3–5), 149–159. https://doi.org/10.1016/j.jog.2007.02.004

Barde-Cabusson, S., Bolós, X., Pedrazzi, D., Lovera, R., Serra, G., Martí, J., & Casas, A. (2013). Electrical resistivity tomography revealing the internal structure of monogenetic volcanoes. *Geophysical Research Letters*, *40*(11), 2544–2549. https://doi.org/10.1002/grl.50538

Bolós, X., Barde-Cabusson, S., Pedrazzi, D., Martí, J., Casas, A., Himi, M., & Lovera, R. (2012). Investigation of the inner structure of La Crosa de Sant Dalmai maar (Catalan volcanic zone, Spain). *Journal of Volcanology and Geothermal Research*, *247–248*, 37–48. https://doi.org/10.1016/j.jvolgeores.2012.08

Bräuer, K., Kämpf, H., Niedermann, S., Strauch, G., & Tesař, J. (2008). The natural laboratory NW Bohemia—Comprehensive fluid studies between 1992 and 2005 used to trace geodynamic processes. *Geochemistry, Geophysics, Geosystems*, *9*(4), Q04018. https://doi.org/10.1029/2007GC001921

Bräuer, K., Kämpf, H., & Strauch, G. (2009). Earthquake swarms in nonvolcanic regions: What fluids have to say. *Geophysical Research Letters*, *36*(17), 17309. https://doi.org/10.1029/2009GL039615

Bräuer, K., Kämpf, H., Strauch, G., & Weise, S. M. (2003). Isotopic evidence (3He/4He, 13CCO2) of fluid triggered intraplate seismicity. *Journal of Geophysical Research*, *108*(B2), 2070. https://doi.org/10.1029/2002JB002077

Brunner, I., Friedel, S., Jacobs, F., & Danckwardt, E. (1999). Investigation of the Tertiary maar structure using three-dimensional resistivity imaging. *Geophysical Journal International*, *136*(3), 771–780. https://doi.org/10.1046/j.1365-246x.1999.00770.x

Büchner, J., Tietz, O., Viereck, L., Suhr, P., & Abratis, M. (2015). Volcanology, geochemistry and age of the Lausitz Volcanic Field. *International Journal of Earth Sciences*, *104*(8), 2057–2083. https://doi.org/10.1007/s00531-015-1165-3

Cajz, V., Rapprich, V., Schnabl, P., & Pécskay, Z. (2009). A proposal on lithostratigraphy of Cenozoic volcanic rocks in Eastern Bohemia. *Geoscience Research Reports*, *49*, 9–14.

Cajz, V., Schnabl, P., Pécskay, Z., Skácelová, Z., Venhodová, D., Šlechta, S., & Čížková, K. (2012). Chronological implications of the paleomagnetic record of the Late Cenozoic volcanic activity along the Moravia-Silesia border (NE Bohemian Massif). *Geologica Carpathica*, *63*(5), 423–435. https://doi.org/10.2478/v10096-012-0033-3

Chulliat, A., Brown, W., Alken, P., Beggan, C., Nair, M., Cox, G., et al. (2020). *The US/UK World magnetic model for 2020–2025: Technical Report*. National Centers for Environmental Information, NOAA. https://doi.org/10.25923/ytk1-yx35

Cockett, R., Kang, S., Heagy, L. J., Pidlisecky, A., & Oldenburg, D. W. (2015). SimPEG: An open source framework for simulation and gradient based parameter estimation in geophysical applications. *Computers & Geosciences*, *85*, 142–154. https://doi.org/10.1016/j.cageo.2015.09.015

Cole, P. D., Guest, J. E., Duncan, A. M., & Pacheco, J.-M. (2001). Capelinhos 1957–1958, Faial, Azores: Deposits formed by an emergent Surtseyan eruption. *Bulletin of Volcanology*, *63*(2–3), 204–220. https://doi.org/10.1007/s004450100136

Cooper, G. R. J., & Cowan, D. R. (2005). Differential reduction to the pole. *Computers & Geosciences*, *31*(8), 989–999. https://doi.org/10.1016/j.cageo.2005.02.005

Fischer, T., Horálek, J., Hrubcová, P., Vavryčuk, V., Bräuer, K., & Kämpf, H. (2014). Intra-continental earthquake swarms in West-Bohemia and Vogtland, a review. *Tectonophysics*, *611*, 1–27. https://doi.org/10.1016/j.tecto.2013.11.001

Fischer, T., Hrubcová, P., Dahm, T., Woith, H., Vylita, T., Ohrnberger, M., et al. (2022). ICDP Eger Rift observatory, magmatic fluids driving the earthquake swarms and deep biosphere—Scientific and technological achievements. *Scientific Drilling*, *31*, 31–49. https://doi.org/10.5194/sd-31-31-2022

Fischer, T., Matyska, C., & Heinicke, J. (2017). Earthquake-enhanced permeability—Evidence from carbon dioxide release following the M_L 3.5 earthquake in West Bohemia. *Earth and Planetary Science Letters*, *460*, 60–67. https://doi.org/10.1016/j.epsl.2016.12.001

Fischer, T., Štěpančíková, P., Karousová, M., Tábořík, P., Flechsig, C., & Gaballah, M. (2012). Imaging the Mariánské Lázně Fault (Czech Republic) by 3-D ground-penetrating radar and electric resistivity tomography. *Studia Geophysica et Geodaetica*, *56*(4), 1019–1036. https://doi.org/10.1007/s11200-012-0825-z

Fischer, T., Vlček, J., & Lanzendörfer, M. (2020). Monitoring crustal CO_2 flow: Methods and their applications to the mofettes in West Bohemia. *Solid Earth*, *11*(3), 983–998. https://doi.org/10.5194/se-11-983-2020

Flechsig, C., Heinicke, J., Mrlina, J., Kämpf, H., Nickschick, T., Schmidt, A., et al. (2015). Integrated geophysical and geological methods to investigate the inner and outer structures of the Quaternary Mýtina maar (W-Bohemia, Czech Republic). *International Journal of Earth Sciences*, *104*(8), 2087–2105. https://doi.org/10.1007/s00531-014-1136-0

Foucher, M. S., Petronis, M. S., Lindline, J., & van Wyk de Vries, B. (2018). Investigating the magmatic plumbing system of a monogenetic scoria cone, a field and laboratory study of the Cienega scoria cone, Cerros del Rio Volcanic Field, New Mexico. *Geochemistry, Geophysics, Geosystems*, *19*(7), 1963–1978. https://doi.org/10.1029/2017gc007222

Gjerløw, E., Höskuldsson, A., & Pedersen, R. B. (2015). The 1732 Surtseyan eruption of Eggøya, Jan Mayen, North Atlantic: Deposits, distribution, chemistry and chronology. *Bulletin of Volcanology*, *77*(2), 1–21. https://doi.org/10.1007/s00445-014-0895-6

Gottsmann, J. (1999). Tephra characteristics and eruption mechanism of the Komorní Hůrka Hill scoria cone, Cheb Basin, Czech Republic. *Geolines*, *9*, 35–40.

Güllü, B., & Kadıoğlu, Y. K. (2019). The petro-chemical properties of Meke and Acıgöl (Karapınar-Konya) volcanites. Pamukkale University. *Journal of Engineering Sciences*, *25*(3), 325–335. https://doi.org/10.5505/PAJES.2018.28159

Günther, T., Rücker, C., & Spitzer, K. (2006). Three-dimensional modelling and inversion of dc resistivity data incorporating topography—II. Inversion. *Geophysical Journal International*, *166*(2), 506–517. https://doi.org/10.1111/j.1365-246X.2006.03011.x

Hintz, A. R., & Valentine, G. A. (2012). Complex plumbing of monogenetic scoria cones: New insights from the Lunar Crater Volcanic Field (Nevada, USA). *Journal of Volcanology and Geothermal Research*, *239*(240), 19–32. https://doi.org/10.1016/j.jvolgeores.2012.06.008

Holub, F. V., Rapprich, V., Erban, V., Pécskay, Z., Mlčoch, B., & Míková, J. (2010). Petrology and geochemistry of the tertiary alkaline intrusive rocks at Doupov, Doupovské hory Volcanic Complex (NW Bohemian Massif). *Journal of Geosciences*, *55*, 251–278. https://doi.org/10.3190/jgeosci.074

Horálek, J., & Fischer, T. (2008). Role of crustal fluids in triggering the West Bohemia/Vogtland earthquake swarms: Just what we know (a review). *Studia Geophysica et Geodaetica*, *52*(4), 455–478. https://doi.org/10.1007/s11200-008-0032-0

Hošek, J., Valenta, J., Rapprich, V., Hroch, T., Turjaková, V., Tábořík, P., & Pokorný, P. (2019). Nově identifikované pleistocenní maary v západních Čechách. *Geoscience Research Reports*, *52*, 97–104.

Hradecký, P. (1994). Volcanology of Železná and Komorní hůrka in Western Bohemia. *Věstník Českého Geologického Ustavu*, *69*, 89–92.

Hrubcová, P., Fischer, T., Rapprich, V., Valenta, J., Tábořík, P., Mrlina, J., et al. (2023). Data for the paper "Two small volcanoes, one inside the other: geophysical and drilling investigation of Bažina maar in western Eger Rift" (Version 2) [Dataset]. Zenodo. https://doi.org/10.5281/ZENODO.7889693

Hrubcová, P., & Geissler, W. H. (2009). The crust-mantle transition and the Moho beneath the Vogtland/West Bohemian region in the light of different seismic methods. *Studia Geophysica et Geodaetica*, *53*(3), 275–294. https://doi.org/10.1007/s11200-009-0018-6

Hrubcová, P., Geissler, W. H., Bräuer, K., Vavryčuk, V., Tomek, Č., & Kämpf, H. (2017). Active magmatic underplating in western Eger Rift, central Europe. *Tectonics*, *36*(12), 2846–2862. https://doi.org/10.1002/2017TC004710

Hrubcová, P., Środa, P., Špičák, A., Guterch, A., Grad, M., Keller, G. R., et al. (2005). Crustal and uppermost mantle structure of the Bohemian Massif based on CELEBRATION 2000 data. *Journal of Geophysical Research*, *110*(B11), B11305. https://doi.org/10.1029/2004JB003080

Hrubcová, P., Vavryčuk, V., Boušková, A., & Horálek, J. (2013). Moho depth determination from waveforms of microearthquakes in the West Bohemia/Vogtland swarm area. *Journal of Geophysical Research*, *118*(1), 120–137. https://doi.org/10.1029/2012JB009360

Keating, G. N., Valentine, G. A., Krier, D. J., & Perry, F. V. (2008). Shallow plumbing systems for small-volume basaltic volcanoes. *Bulletin of Volcanology*, *70*(5), 563–582. https://doi.org/10.1007/s00445-007-0154-1

Kiyosugi, K., Horikawa, Y., Nagao, T., Itaya, T., Connor, C. B., & Tanaka, K. (2014). Scoria cone formation through a violent Strombolian eruption: Irao volcano, SW Japan. *Bulletin of Volcanology*, *76*(1), 781. https://doi.org/10.1007/s00445-013-0781-7

Kokelaar, B. P. (1983). The mechanism of Surtseyan volcanism. *Journal of the Geological Society*, *140*(6), 939–944. https://doi.org/10.1144/gsjgs.140.6.0939

Latutrie, B., & Ross, P.-S. (2019). Transition zone between the upper diatreme and lower diatreme: Origin and significance at Round Butte, Hopi Buttes volcanic field, Navajo Nation, Arizona. *Bulletin of Volcanology*, *81*(4), 26. https://doi.org/10.1007/s00445-019-1285-x

Latutrie, B., & Ross, P.-S. (2020). Phreatomagmatic vs magmatic eruptive styles in maar-diatremes: A case study at Twin Peaks, Hopi Buttes volcanic field, Navajo Nation, Arizona. *Bulletin of Volcanology*, *82*(3), 28. https://doi.org/10.1007/s00445-020-1365-y

Latutrie, B., & Ross, P.-S. (2021). What lithic clasts and lithic-rich facies can tell us about diatreme processes: An example at Round Butte, Hopi Buttes volcanic field, Navajo Nation, Arizona. *Journal of Volcanology and Geothermal Research*, *411*, 107150. https://doi.org/10.1016/j.jvolgeores.2020.107150

Läuchli, B., Augustinus, P. C., Peti, L., & Hopkins, J. L. (2021). Composite development and stratigraphy of the Onepoto maar lake sediment sequence (Auckland Volcanic Field, New Zealand). *Scientific Drilling*, *29*, 19–37. https://doi.org/10.5194/sd-29-19-2021

Lefebvre, N. S., White, J. D. L., & Kjarsgaard, B. A. (2013). Unbedded diatreme deposits reveal maar-diatreme-forming eruptive processes: Standing Rocks West, Hopi Buttes, Navajo Nation, USA. *Bulletin of Volcanology*, *75*(8), 1–17. https://doi.org/10.1007/s00445-013-0739-9

Lorenz, V., & Kurszlaukis, S. (2007). Root zone processes in the phreatomagmatic pipe emplacement model and consequences for the evolution of maar-diatreme volcanoes. *Journal of Volcanology and Geothermal Research*, *159*(1–3), 4–32. https://doi.org/10.1016/j.jvolgeores.2006.06.019

Martin, U., & Németh, K. (2004). Mio/pliocene phreatomagmatic volcanism in the Western Pannonian Basin. *Geologica Hungarica*, *26*(12–56). 963 671 238 7.

McPhie, J., Doyle, M., & Allen, R. (1993). *Volcanic textures, a guide to the interpretation of textures in volcanic rocks* (p. 198). CODES, Hobart.

Mlčoch, B., & Konopásek, J. (2010). Pre-Late Carboniferous geology along the contact of the Saxothuringian and Teplá-Barrandian zones in the area covered by younger sediments and volcanics (western Bohemian Massif, Czech Republic). *Journal of Geosciences*, *55*, 81–94. https://doi.org/10.3190/jgeosci.068

Mrlina, J., Kämpf, H., Geissler, W. H., & vanden Boogart, P. (2007). Assumed Quaternary maar structure at the Czech/German boundary between Mýtina and Neualbenreuth (western Eger Rift, central Europe): Geophysical, petrochemical and geochronological indications. *Zeitschrift für Geologische Wissenschaften*, *35*(4–5), 213–230.

Mrlina, J., Kämpf, H., Kroner, C., Mingram, J., Stebich, M., Brauer, A., et al. (2009). Discovery of the first Quaternary maar in the Bohemian Massif, Central Europe, based on combined geophysical and geological surveys. *Journal of Volcanology and Geothermal Research*, *182*(1–2), 97–112. https://doi.org/10.1016/j.jvolgeores.2009.01.027

Mrlina, J., Kämpf, H., Polák, V., & Seidl, M. (2019). Indication of two unknown Quaternary maar volcanoes near Liba in West Bohemia based on gravity survey. *Bulletin of Brown Coal*, *2*, 19–23. (in Czech, English abstract).

Muñoz, G., Weckmann, U., Pek, J., Kováčiková, S., & Klanica, R. (2018). Regional two-dimensional magnetotelluric profile in West Bohemia/Vogtland reveals deep conductive channel into the earthquake swarm region. *Tectonophysics*, *727*, 1–11. https://doi.org/10.1016/j.tecto.2018.01.012

Murtagh, R. M., & White, J. D. (2013). Pyroclast characteristics of a subaqueous to emergent Surtseyan eruption, Black Point volcano, California. *Journal of Volcanology and Geothermal Research*, *267*, 75–91. https://doi.org/10.1016/j.jvolgeores.2013.08.015

Németh, K., Cronin, S. J., Charley, D., Harrison, M., & Garae, E. (2006). Exploding lakes in Vanuatu—"Surtseyan-style" eruptions witnessed on Ambae Island. *Episodes*, *29*(2), 87–92. https://doi.org/10.18814/epiiugs/2006/v29i2/002

Németh, K., Goth, K., Martin, U., Csillag, G., & Suhr, P. (2008). Reconstructing paleoenvironment, eruption mechanism and paleomorphology of the Pliocene Pula maar, (Hungary). *Journal of Volcanology and Geothermal Research*, *177*(2), 441–456. https://doi.org/10.1016/j.jvolgeores.2008.06.010

Németh, K., Kereszturi, G., Agustin-Flores, J., Briggs, R., Cronin, S. J., Lindsay, J. M., et al. (2012). Field guide: Monogenetic volcanism of the South Auckland and Auckland volcanic fields. In *Paper presented at 4th International Maar Conference, Auckland, New Zealand, February 20–24, 2012* (pp. 1–70).

Németh, K., & Kósik, S. (2020a). Review of explosive hydrovolcanism. *Geosciences*, *10*(2), 44. https://doi.org/10.3390/geosciences10020044

Németh, K., & Kósik, S. (2020b). The role of hydrovolcanism in the formation of the Cenozoic monogenetic volcanic fields of Zealandia. *New Zealand Journal of Geology and Geophysics*, *63*(4), 402–427. https://doi.org/10.1080/00288306.2020.1770304

Oms, O., Bolós, X., Barde-Cabusson, S., Martí, J., Casas, A., Lovera, R., et al. (2015). Structure of the Pliocene Camp dels Ninots maar-diatreme (Catalan volcanic zone, NE Spain). *Bulletin of Volcanology*, *77*(11), 1–13. https://doi.org/10.1007/s00445-015-0982-3

Peti, L., & Augustinus, P. C. (2019). Stratigraphy and sedimentology of the Orakei maar lake sediment sequence (Auckland Volcanic Field, New Zealand). *Scientific Drilling*, *25*, 47–56. https://doi.org/10.5194/sd-25-47-2019

Petronis, M. S., Delcamp, A., & van Wyk de Vries, B. (2013). Magma emplacement into the Lemptégy scoria cone (Chaîne Des Puys, France) explored with structural, anisotropy of magnetic susceptibility, and paleomagnetic data. *Bulletin of Volcanology*, *75*(10), 1–22. https://doi.org/10.1007/s00445-013-0753-y

Petronis, M. S., Valenta, J., Rapprich, V., Lindline, J., Heizler, M., van Wyk de Vries, B., et al. (2018). Emplacement history of the Miocene Zebín tuff cone (Czech Republic) revealed from ground geophysics, anisotropy of magnetic susceptibility, paleomagnetic, and $^{40}Ar/^{39}Ar$ geochronology data. *Geochemistry, Geophysics, Geosystems*, *19*(10), 3764–3792. https://doi.org/10.1029/2017gc007324

Platz, A., Weckmann, U., Pek, J., Kováčiková, S., Klanica, R., Mair, J., & Aleid, B. (2022). 3D imaging of the subsurface electrical resistivity structure in West Bohemia/Upper Palatinate covering mofettes and Quaternary volcanic structures by using Magnetotellurics. *Tectonophysics*, *833*, 229353. https://doi.org/10.1016/j.tecto.2022.229353

Plomerová, J., Munzarová, H., Vecsey, L., Kissling, E., Achauer, U., & Babuška, V. (2016). Cenozoic volcanism in the Bohemian Massif in the context of *P* and *S* velocity high-resolution teleseismic tomography of the upper mantle. *Geochemistry, Geophysics, Geosystems*, *17*(8), 3326–3349. https://doi.org/10.1002/2016gc006318

Prodehl, C., Mueller, S., & Haak, V. (1995). The European Cenozoic rift system. In K. H. Olsen (Ed.), *Continental rifts, evolution, structure, tectonics. Developments in Geotectonics*, (Vol. 25, pp. 133–212). Elsevier.

Rajchl, M., Uličný, D., Grygar, R., & Mach, K. (2009). Evolution of basin architecture in an incipient continental rift: The Cenozoic most basin, Eger Graben (central Europe). *Basin Research*, *21*(3), 269–294. https://doi.org/10.1111/j.1365-2117.2008.00393.x

Rapprich, V., Cajz, V., Košťák, M., Pécskay, Z., Řídkošil, T., Raška, P., & Radoň, M. (2007). Reconstruction of eroded monogenic Strombolian cones of Miocene age, a case study on character of volcanic activity of the Jičín Volcanic Field (NE Bohemia) and subsequent erosional rates estimation. *Journal of Geosciences*, *52*, 169–180. https://doi.org/10.3190/jgeosci.011

Rapprich, V., Lisec, M., Fiferna, P., & Závada, P. (2017). Application of modern technologies in popularization of the Czech volcanic geoheritage. *Geoheritage*, *9*(3), 413–420. https://doi.org/10.1007/s12371-016-0208-x

Rapprich, V., Valenta, J., Brož, M., Kadlecová, E., van Wyk de Vries, B., Petronis, M. S., & Rojík, P. (2019). A crucial site in the argument between Neptunists and Plutonists, reopening of the historical adit in the Komorní hůrka (Kammerbühl) volcano after 180 years. *Geoheritage*, *11*(2), 347–358. https://doi.org/10.1007/s12371-018-0286-z

Rohrmüller, J., Kämpf, H., Geiß, E., Großmann, J., Grun, I., Mingram, J., et al. (2018). Reconnaissance study of an inferred Quaternary maar structure in the western part of the Bohemian Massif near Neualbenreuth, NE-Bavaria (Germany). *International Journal of Earth Sciences*, *107*(4), 1381–1405. https://doi.org/10.1007/s00531-017-1543-0

Ross, P. S., Delpit, S., Haller, M. J., Németh, K., & Corbella, H. (2011). Influence of the substrate on maar-diatreme volcanoes—An example of a mixed setting from the Pali Aike volcanic field, Argentina. *Journal of Volcanology and Geothermal Research*, *201*(1–4), 253–271. https://doi.org/10.1016/j.jvolgeores.2010.07.018

Rücker, C., Günther, T., & Spitzer, K. (2006). Three-dimensional modelling and inversion of dc resistivity data incorporating topography—I. Modeling. *Geophysical Journal International*, *166*(2), 495–505. https://doi.org/10.1111/j.1365-246X.2006.03010.x

Sirocko, F., Dietrich, S., Veres, D., Grootes, P. M., Schaber-Mohr, K., Seelos, K., et al. (2013). Multi-proxy dating of Holocene maar lakes and Pleistocene dry maar sediments in the Eifel, Germany. *Quaternary Science Reviews*, *62*, 56–76. https://doi.org/10.1016/j.quascirev.2012.09.011

Skácelová, Z., Rapprich, V., Valenta, J., Hartvich, F., Šrámek, J., Radoň, M., et al. (2010). Geophysical research on structure of partly eroded maar volcanoes, Miocene Hnojnice and Oligocene Rychnov volcanoes (northern Czech Republic). *Journal of Geosciences*, *55*, 333–345. https://doi.org/10.3190/jgeosci.072

Skála, R., Ulrych, J., Ackerman, L., Jelínek, E., Dostál, J., Hegner, E., & Řanda, Z. (2014). Tertiary alkaline Roztoky intrusive complex, České středohoří Mts., Czech Republic, petrogenetic characteristics. *International Journal of Earth Sciences*, *103*(5), 1233–1262. https://doi.org/10.1007/s00531-013-0948-7

Sohn, Y. K., & Park, K. H. (2005). Composite tuff ring/cone complexes in Jeju Island, Korea: Possible consequences of substrate collapse and vent migration. *Journal of Volcanology and Geothermal Research*, *141*(1–2), 157–175. https://doi.org/10.1016/j.jvolgeores.2004.10.003

Soleymanzadeh, A., Kolahkaj, P., Kord, S., & Monjezi, M. (2021). A new technique for determining water saturation based on conventional logs using dynamic electrical rock typing. *Journal of Petroleum Science and Engineering*, *196*, 107803. https://doi.org/10.1016/j.petrol.2020.107803

Špičáková, L., Uličný, D., & Koudelková, G. (2000). Tectonosedimentary evolution of the Cheb Basin (NW Bohemia, Czech Republic) between late Oligocene and Pliocene, a preliminary note. *Studia Geophysica et Geodaetica*, *44*(4), 556–580. https://doi.org/10.1023/a:1021819802569

Swanson, E. R. (1989). A new type of maar volcano from the state of durango-the El Jagüey-La Breña complex reinterpreted. *Revista Mexicana de Ciencias Geológicas*, *8*(2), 243–247.

Taddeucci, J., Edmonds, M., Houghton, B., James, M. R., & Vergniolle, S. (2015). Hawaiian and Strombolian eruptions. *The Encyclopedia of Volcanoes*, 485–503. https://doi.org/10.1016/b978-0-12-385938-9.00027-4

Thordarson, T., & Sigmarsson, O. (2009). *Effusive activity in the 1963–1967 Surtsey eruption, Iceland: Flow emplacement and growth of small lava shields*. *Studies in Volcanology: the Legacy of George Walker* (Vol. 2, pp. 53–84). Special Publication of IAVCEI.

Ulrych, J., Ackerman, L., Balogh, K., Hegner, E., Jelínek, E., Pécskay, Z., et al. (2013). Plio-Pleistocene basanitic and melilititic series of the Bohemian Massif, K–Ar ages, major/trace element and Sr–Nd isotopic data. *Chemie der Erde—Geochemistry*, *73*(4), 429–450. https://doi.org/10.1016/j.chemer.2013.02.001

Ulrych, J., Dostál, J., Adamovič, J., Jelínek, E., Špaček, P., Hegner, E., & Balogh, K. (2011). Recurrent Cenozoic volcanic activity in the Bohemian Massif (Czech Republic). *Lithos*, *123*(1–4), 133–144. https://doi.org/10.1016/j.lithos.2010.12.008

Ulrych, J., Krmíček, L., Tomek, Č., Lloyd, F. E., Ladenberger, A., Ackerman, L., & Balogh, K. (2016). Petrogenesis of Miocene alkaline volcanic suites from western Bohemia: Whole rock geochemistry and Sr–Nd–Pb isotopic signatures. *Chemie Der Erde—Geochemistry*, *76*(1), 77–93. https://doi.org/10.1016/j.chemer.2015.11.003

Ulrych, J., Lloyd, F. E., & Balogh, K. (2003). Age relations and geochemical constraints of Cenozoic alkaline volcanic series in W Bohemia: A review. *Geolines*, *15*, 168–180.

Valenta, J., Rapprich, V., Skácelová, Z., Gaždová, R., & Fojtíková, L. (2014). The newly discovered Neogene maar volcano near the Mariánské Lázně, Western Bohemia. *Acta Geodynamica et Geomaterialia*, *11*(2), 107–116. https://doi.org/10.13168/AGG.2013.0061

Valenta, J., Rapprich, V., Stárková, M., Skácelová, Z., Fojtíková, L., Staněk, F., & Balek, J. (2014). Problems and challenges in detection of pre-Mesozoic maar volcanoes, example from the Principálek volcano in the Permian Krkonoše Piedmont basin. *Journal of Geosciences*, *59*, 169–181. https://doi.org/10.3190/jgeosci.170

Valentine, G. A., & van Wyk de Vries, B. (2014). Unconventional maar diatreme and associated intrusions in the soft sediment-hosted Mardoux structure (Gergovie, France). *Bulletin of Volcanology*, *76*(3), 807. https://doi.org/10.1007/s00445-014-0807-9

Weinlich, F. H., Bräuer, K., Kämpf, H., Strauch, G., Tesar, J., & Weise, S. M. (1999). An active subcontinental mantle volatile system in the western Eger Rift, central Europe: Gas flux, isotopic (He, C, and N) and compositional fingerprints. *Geochimica et Cosmochimica Acta*, *63*(21), 3653–3671. https://doi.org/10.1016/s0016-7037(99)00187-8

Wenger, E., Büchner, J., Tietz, O., & Mrlina, J. (2017). The polycyclic Lausche volcano (Lausitz volcanic field) and its message concerning landscape evolution in the Lausitz mountains (northern Bohemian Massif, central Europe). *Geomorphology*, *292*, 193–210. https://doi.org/10.1016/j.geomorph.2017.04.021

White, J. D. L. (1990). Depositional architecture of a maar-pitted playa: Sedimentation in the Hopi Buttes volcanic field, northeastern Arizona, USA. *Sedimentary Geology*, *67*(1–2), 55–84. https://doi.org/10.1016/0037-0738(90)90027-Q

White, J. D. L., & Ross, P.-S. (2011). Maar-diatreme volcanoes, a review. *Journal of Volcanology and Geothermal Research*, *201*(1–4), 1–29. https://doi.org/10.1016/j.jvolgeores.2011.01.010

Wilson, M., & Downes, H. (1991). Tertiary—Quaternary extension-related alkaline magmatism in western and central Europe. *Journal of Petrology*, *32*(4), 811–849. https://doi.org/10.1093/petrology/32.4.811

Zolitschka, B., Anselmetti, F., Ariztegui, D., Corbella, H., Francus, P., Lücke, A., et al. (2013). Environment and climate of the last 51,000 years—New insights from the Potrok aike maar lake sediment archive drilling project (PASADO). *Quaternary Science Reviews*, *71*, 1–12. https://doi.org/10.1016/j.quascirev.2012.11.024